Identification of overlapping and distinct mural cell populations during early embryonic development

Sarah Colijn[1#], Miku Nambara[1#], and Amber N. Stratman[1*]

[1]Department of Cell Biology and Physiology, Washington University in St. Louis, School of Medicine, St. Louis, MO 63110

[#]Contributed equally

[*]Correspondence: a.stratman@wustl.edu (ANS), 1-314-273-7928

Running Title: *pdgfrb* and *tagln* in zebrafish embryos

Keywords**:** mural cell progenitor, vSMC, pericyte, perivascular cells, hypochord, sclerotome, zebrafish

Summary Statement:

Detailed analysis of *pdgfrb*/*tagln* vascular expression patterns in embryonic zebrafish reveals novel regions of *tagln*-positive populations such as the hypochord and a mural cell progenitor population adjacent to the midline.

Abstract:

Mural cells are an essential perivascular cell population that associate with blood vessels and contribute to vascular stabilization and tone. In the embryonic zebrafish vasculature, *pdgfrb* and *tagln* are commonly used as markers for identifying pericytes and vascular smooth muscle cells (vSMCs). However, the expression patterns of these markers used in tandem have not been fully described. Here, we used the *Tg(pdgfrb:Gal4FF; UAS:RFP)* and *Tg(tagln:NLS-EGFP)* transgenic lines to identify single- and double-positive perivascular populations in the cranial, axial, and intersegmental vessels between 1 and 5 days post-fertilization. From this comparative analysis, we discovered two novel regions of *tagln*-positive cell populations that have the potential to function as mural cell precursors. Specifically, we found that the hypochord—a reportedly transient structure—contributes to *tagln*-positive cells along the dorsal aorta. We also identified a unique sclerotome-derived mural cell progenitor population that resides along the midline between the neural tube and notochord and contributes to intersegmental vessel mural cell coverage. Together, our findings highlight the variability and versatility of tracking *pdgfrb* and *tagln* expression in mural cells of the developing zebrafish embryo.

39 **Introduction:**

40 In vertebrate development, early blood vessels are initially comprised of a single
41 layer of endothelial cells—which then recruit mural cells to assist in basement membrane
42 deposition, vessel contractility, and cellular communication (Armulik et al., 2005). Mural
43 cells can vary widely in morphology and gene expression patterns depending on vessel
44 type, vascular bed, tissue origin, differentiation status, developmental stage, and more
45 (Donadon and Santoro, 2021, Owens et al., 2004, Holm et al., 2018). Types of mural cells
46 include pericytes—which are associated with smaller vessels such as capillaries—and
47 vascular smooth muscle cells (vSMCs) on larger vessels. vSMCs will accumulate on
48 arteries and—to a lesser extent—on veins during vascular development to provide tensile
49 strength and promote basement membrane deposition (Stratman et al., 2017). Due to the
50 diverse properties of mural cells, different gene expression profiles can be used to identify
51 mural cell types along various regions of the vasculature. Therefore, identification of
52 appropriate cellular markers for distinct developmental stages is necessary for the study
53 of vessel stabilization in different vascular beds.

54 In the embryonic zebrafish, platelet-derived growth factor receptor beta (*pdgfrb*)
55 and transgelin (*tagln*) are commonly used as markers to identify pericytes and vSMCs.
56 However, the temporal expression patterns of these markers used in tandem has not
57 been fully described. Pdgfrb—a surface receptor for the chemoattractant ligands of the
58 Pdgf family—is used as a marker for pericytes and immature vSMCs (Hellstrom et al.,
59 1999, Armulik et al., 2005, Ando et al., 2021b). Pdgfrb has been shown to be required for
60 mural cell expansion both embryonically and postnatally (Leonard et al., 2022, Ando et
61 al., 2021b, Stratman et al., 2020). Cranial and cardiac neural crest cells also express
62 Pdgfrb and have the capacity to become mural cells in addition to giving rise to other
63 mesenchymal cell populations (Smith and Tallquist, 2010, Majesky, 2007, Ando et al.,
64 2016). Some mature mural cells—such as pericytes—continue to express Pdgfrb, though
65 less than 1% of Pdgfrb-positive cells in a zebrafish larvae at 5 days post-fertilization (dpf)
66 are pericytes (Shih et al., 2021). This suggests that most Pdgfrb-positive cells in early
67 development are progenitors for diverse cell populations.

68 Tagln (or SM22)—an actin-binding protein from the calponin family—is commonly
69 used to identify mature, contractile vSMCs (Chakraborty et al., 2019, Santoro et al.,

2009). Tagln and other actin-binding proteins confer contractile function to mature mural cells, allowing them to regulate vascular tone and blood pressure (Rensen et al., 2007). During development, Tagln is also expressed in intestinal smooth muscle, cardiac muscle, and skeletal muscle cells (Seiler et al., 2010, Li et al., 1996), though these muscle cells can be distinguished from vSMCs by observing cellular morphology and proximity to the vasculature. Altogether, this suggests that the *pdgfrb* and *tagln* reporters can be used to identify mural cells and their differentiation status by tracking single- versus double-positive cells in discrete vascular beds over the course of early development.

In this report, we use *Tg(pdgfrb:Gal4FF; UAS:RFP)* and *Tg(tagln:NLS-EGFP)* transgenic lines to identify single- and double-positive pericytes/vSMCs in the cranial, axial, and intersegmental vessels (ISVs) at 1 to 5 dpf. Through this study, we have uncovered two novel sites of *tagln*-positive cell populations that have the potential to function as mural cell precursors in the zebrafish trunk. First, we found that the hypochord—a reportedly transient structure present in fish and amphibians—contributes to *tagln*-positive cells along the dorsal aorta. Second, we identified a sclerotome-derived mural cell progenitor population that resides along the midline at the notochord-neural tube interface and contributes to ISV mural cell coverage. These findings highlight unexpected and nuanced gene expression patterns across perivascular cell maturation.

Results:

pdgfrb and *tagln* transgenic reporter lines

To visualize mural cells in the zebrafish embryo, we crossed the established transgenic lines *TgBAC(pdgfrb:Gal4FF)*^{ncv24}, *Tg(5xUAS:RFP)*^{zf83}, and *Tg(tagln:NLS-EGFP-2A-CFP-FTASE)*^{y450} to generate embryos that were heterozygous carriers for each transgene. Expression of both *pdgfrb* and *tagln* were notable at all embryonic stages analyzed—with the brightest signal for *pdgfrb* visible in the anterior and cranial regions, and *tagln* in the skeletal muscle of the trunk and later in the intestinal compartment (Fig. S1).

The *pdgfrb* reporter line utilizes the Gal4/UAS system (Ando et al., 2016)—designated as *Tg(pdgfrb:Gal4FF; UAS:RFP)* in this report—and mosaic fluorescence was occasionally observed during screening; embryos with the least mosaicism were selected

101 for use. The *tagln* reporter line—designated as *Tg(tagln:NLS-EGFP)*—contains a nuclear
102 localization signal that allows for GFP to be concentrated in the nucleus (Stratman et al.,
103 2017), a modification that facilitates the identification of individual *tagln*-positive cells in
104 regions with dense *tagln* expression. With this tool, our study provides a unique approach
105 to tracking *pdgfrb* and *tagln* localization in the zebrafish.
106
107 **Imaging the mural cells of the cranial vasculature**
108 Development of the zebrafish cranial vasculature has been thoroughly mapped
109 through numerous studies. This process involves the formation of the primordial hind- and
110 midbrain channels (PHBC/PMBC) and the lateral dorsal aorta (LDA) by 1 dpf, the growth
111 of the middle cerebral vein (MCeV), metencephalic artery (MtA), basilar artery (BA), and
112 Circle of Willis (CoW) by 1.5 dpf, and the sprouting and fusion of various central arteries
113 (CtAs) from the PHBC to the BA by 2 dpf (Ulrich et al., 2011, Fujita et al., 2011, Isogai et
114 al., 2001). These vessels continue to remodel, grow, and stabilize, though the patterning
115 remains mostly intact from 6 dpf and beyond (Isogai et al., 2001).
116 Mural cell coverage of the cranial vessels has also been frequently studied, with
117 the common understanding being that neural crest-derived *pdgfrb*-positive pericytes are
118 the predominant mural cell in the mid- and hindbrain prior to 5 dpf (Ando et al., 2019,
119 Ando et al., 2016, Ando et al., 2021a, Wang et al., 2014). Interestingly, Ando et al have
120 shown that some mural cells in the hindbrain are derived from mesoderm. Specifically,
121 *pdgfrb*-positive cells surrounding the PHBC at 1 dpf are purportedly mesoderm-derived
122 mesenchyme; these cells then increase *pdgfrb* expression, migrate to CtAs, and
123 eventually acquire vSMC markers—such as *tagln*—at 5 dpf (Ando et al., 2016, Ando et
124 al., 2021a). Prior to 5 dpf, vSMC markers are sparse in the cranial vessels, with less than
125 10% of mural cells on the CtAs expressing *tagln* by 5 dpf (Ando et al., 2019).
126 In our *Tg(tagln:NLS-EGFP); Tg(pdgfrb:Gal4FF; UAS:RFP)* embryos, as expected,
127 *pdgfrb* was the predominant marker of cranial mural cells between 1 and 5 dpf (Figs 1A-
128 J; S2A-K). At 1 dpf, *pdgfrb*-positive cells were loosely associated with the PHBC (Fig.
129 1B)—corroborating previous data (Ando et al., 2021a, Ando et al., 2016)—and with the
130 MtA and MCeV (Fig. S2B,C). Based on the current understanding of the literature, these
131 early *pdgfrb*-positive cells are likely a combination of neural crest and mesoderm-derived

132 mesenchyme that have the potential to migrate to the vessels and continue to mature into
133 mural cells throughout development.
134 After 1 dpf, *pdgfrb*-positive cells slowly accumulate on the CoW and CtAs until 5
135 dpf, the latest stage analyzed (Figs 1C-J; S2D-K). A single *pdgfrb*/*tagln* double-positive
136 cell can be seen at 4 dpf on the middle mesencephalic central artery (MMCtA; Fig. 1H,
137 inset). However, throughout this region, *tagln*-positive cells were extremely sparse at all
138 developmental stages assessed, consistent with previous reports that vSMC markers
139 such as *tagln* are not prevalent in cranial mural cells prior to 4 dpf. These results indicate
140 that *pdgfrb* is the predominant mural cell marker along embryonic cranial vessels, though
141 a small proportion of these cells—particularly on the arteries—can mature into
142 *pdgfrb*/*tagln* double-positive vSMCs by 5 dpf.
143
144 **Imaging the mural cells of the axial vasculature**
145 The main axial vessels—i.e. dorsal aorta (DA) and posterior cardinal vein (PCV)
146 in the anterior trunk and the caudal artery (CA) and caudal vein (CV) in the tail—are some
147 of the first vessels to form prior to the onset of circulation at 1 dpf (Isogai et al., 2001).
148 The mural cells that accumulate on the ventral side of the DA have been well-described;
149 *pdgfrb*-positive cells begin to accumulate at 1.5 dpf and then acquire the vSMC marker
150 *tagln* at 3 dpf (Ando et al., 2021a, Stratman et al., 2017, Ando et al., 2016). Approximately
151 25% of vSMCs on the ventral side of the DA are reported to be *pdgfrb*/*tagln* double-
152 positive by 5 dpf (Ando et al., 2019).
153 The mural cells that cover the dorsal side of the DA are not as well-defined.
154 Intriguingly, the mural cells that accumulate on the dorsal and ventral sides of the DA are
155 initially derived from different mesodermal origins in mice (Wasteson et al., 2008). This
156 lineage difference has not been definitively shown in zebrafish. However, there are clear
157 distinctions between the cells that initially populate the dorsal versus ventral sides of the
158 DA in zebrafish embryos—with the mural cells on the dorsal side of the DA reported to
159 express *tagln* but not *pdgfrb* (Ando et al., 2016).
160 By tracking the expression of *pdgfrb* and *tagln* in vSMCs on the DA, PCV, CA, and
161 CV, we identify the hypochord as a novel source of *tagln*-positive cells on the dorsal side
162 of the DA and CA (Fig. 2). We also corroborate the previous findings regarding vSMC

163 expression patterns on the ventral side of the DA, and observe a slow accumulation of
164 *pdgfrb* single-positive cells on the PCV and CV between 1 to 5 dpf (Fig. 2). Finally, we
165 find that accumulation and maturation of these mural cells occurs in an anterior to
166 posterior fashion, with mural cells on the anterior DA and PCV maturing one to two days
167 earlier than the mural cells of the posterior CA and CV (Fig. 2).

168 To begin, we analyzed *pdgfrb* and *tagln* expression in mural cells of the anterior
169 DA and PCV in *Tg(tagln:NLS-EGFP); Tg(pdgfrb:Gal4FF; UAS:RFP)* embryos between 1
170 to 5 dpf (Fig. 3A-I). We identified the hypochord at 1 dpf as the *pdgfrb*-positive structure
171 immediately dorsal to the DA that runs along the midline (Fig. 3A). The hypochord is a
172 reportedly transient, rod-like structure—only one cell in width and height—that resides
173 beneath the notochord and assists in the formation and patterning of the DA (Eriksson
174 and Löfberg, 2000, Cleaver et al., 2000, Löfberg and Collazo, 1997). Once the DA is
175 formed, the hypochord cells are reported to delaminate and degenerate—in part due to
176 apoptosis (Löfberg and Collazo, 1997, Cleaver et al., 2000)—then by 2.5 dpf either
177 disappear or become indistinguishable from the cells that surround the DA in the zebrafish
178 embryo (Eriksson and Löfberg, 2000).

179 *pdgfrb* expression in the hypochord has been previously reported, in addition to
180 *pdgfrb* expression in the floor plate—the structure that sits on the ventral side of the neural
181 tube (Ando et al., 2019, Ando et al., 2016, Wiens et al., 2010). We found that in addition
182 to *pdgfrb*, the hypochord also expresses *tagln* at the 1 dpf stage (Fig. 3A,F). At 2 dpf, the
183 hypochord cells began to delaminate, as evidenced by the elongating nuclei (Fig. 3B). At
184 3 dpf, when the hypochord is allegedly absent from the anterior trunk (Eriksson and
185 Löfberg, 2000), we observed that the *tagln*-positive cells persist and begin to decrease
186 *pdgfrb* expression (Fig. 3C,F). By 4 dpf, these cells were *tagln* single-positive, with
187 noticeably fewer nuclei visible per vessel length (Fig. 3D,F; Movie 1), indicating that a
188 portion of hypochord cells do degenerate after delamination. However, a portion of
189 elongated *tagln*-positive cells were still present at 5 dpf (Fig. 3E,F), and Ando et al reports
190 observing these *tagln* single-positive cells above the DA as late as 7 dpf (Ando et al.,
191 2016).

192 To confirm that these hypochord-derived cells are maintained—and that they are
193 not ventral vSMCs that have migrated to the dorsal side of the DA—we used a

194 sclerotome-marker twist family bHLH transcription factor 1a (*twist1a*) transgenic line to
195 distinguish their origin (Stratman et al., 2017). The hypochord—in addition to the
196 notochord and floor plate—has been shown to be derived from the multipotent midline
197 progenitor cells in the dorsal organizer or the tailbud (Row et al., 2016, Latimer and Appel,
198 2006). Thus, hypochord cells maintain distinct origins from sclerotome cells, which
199 emerge from the somites (Tani et al., 2020). Indeed, we found that the *tagln* single-
200 positive cells on the dorsal side of the DA are not sclerotome-derived, unlike the vSMCs
201 on the ventral side of the DA (Fig. S3A-F). Altogether, these results suggest that the
202 hypochord is the source of the *tagln* single-positive cells that reside on the dorsal side of
203 the DA. This also indicates that the cells of the hypochord are not entirely transient as
204 previously assumed, but instead a portion reprogram their cellular function and
205 morphology after the DA has been appropriately oriented.

206 We next observed the development of the mural cells on the ventral side of the
207 DA. While the hypochord-derived cells on the dorsal side of the DA flattened and
208 elongated over time, the vSMCs on the ventral side were more globular (Fig. 3A-E).
209 *pdgfrb* single-positive vSMCs were observed beginning at 2 dpf, where they then
210 expanded in number and increased expression of *tagln* (Fig. 3A-E,G). By 5 dpf,
211 *pdgfrb*/*tagln* double-positive cells accounted for approximately 60% of ventral vSMCs,
212 and no *tagln* single-positive cells were detected. These data are consistent with previous
213 reports of vSMCs on the ventral side of the DA, though we observe a higher percentage
214 of double-positive vSMCs (60% versus 25%) by 5 dpf (Ando et al., 2019, Ando et al.,
215 2016, Ando et al., 2021a).

216 Furthermore, we detected *pdgfrb* single-positive cells associated with the PCV as
217 early as 1 dpf—though these cells were sparse—followed by the slow and sporadic
218 accumulation of *pdgfrb*-positive cells until 5 dpf (Fig. 3A-E,H). This timing is earlier than
219 suggested in previous reports where *pdgfrb* expression was undetectable in cells around
220 the PCV prior to 7 dpf (Ando et al., 2016). Stratman et al describes a small number of
221 *tagln*-positive cells on the PCV around 4 dpf (Stratman et al., 2017). Similarly, we saw
222 low numbers of weak *tagln*-positive cells beginning at 3 dpf, though these cells were less
223 common than *pdgfrb* single-positive cells (Fig. 3H). These data indicate that mural cells
224 of the PCV associate and mature at much later developmental stages than aortic vSMCs.

225 In the posterior trunk region, mural cells of the CA and CV associate with vessels
226 and pattern similarly to the anterior mural cells but on a delayed time course (Fig. 4A-I).
227 At 1 dpf, the hypochord cells were block-like and were still distinguishable as hypochord
228 cells by 2 dpf (Fig. 4A,B,F). This was expected, as the hypochord "disappears" in an
229 anterior to posterior fashion (Eriksson and Löfberg, 2000), and is evident at 2 dpf in the
230 posterior region even when it is no longer detectable in the anterior region. We saw the
231 hypochord cells had begun to delaminate by 3 dpf (Fig. 4C), at which point they appeared
232 comparable to the 2 dpf hypochord cells in the anterior region (Fig. 3B). While the cells
233 then began turning off *pdgfrb*, only about a third of hypochord-derived cells in the posterior
234 trunk were *tagln* single-positive by 5 dpf (Fig. 4C-F), indicating a delay in hypochord
235 reprogramming compared to the anterior hypochord.
236 Furthermore, the ventral side of the CA began acquiring *pdgfrb* single-positive cells
237 at 2 dpf—similar to the DA—but they did not begin co-expressing *tagln* until 5 dpf (Fig.
238 4B-E,G). This amounted to a 2-day delay in mural cell development compared to the
239 anterior region (Fig. 3G). Finally, mural cell coverage of the CV was particularly sparse
240 (Fig. 4A-E,H), with half as many cells associated with the CV compared to the PCV at the
241 same developmental stage (Fig. 3H). These data indicate that association and maturation
242 of vSMCs on the main axial vessels occurs in an anterior to posterior fashion across time.
243 Of note, weak *tagln* expression was detected in endothelial cells of the axial
244 vasculature (Fig. S4A,B), which is consistent with previous reports that the endothelium
245 can express low levels of *tagln* (Chakraborty et al., 2019, Tsuji-Tamura et al., 2021).
246 Despite this, *tagln* expression in the endothelial cells was easily distinguishable from
247 vSMCs; therefore, it did not confound the mural cell counts of the axial vessels.
248
249 **Imaging the mural cells of the intersegmental vessels (ISVs)**
250 We next analyzed the mural cell populations surrounding the ISVs of the trunk
251 region. At 1 dpf, arterial ISVs (aISVs) begin to sprout from the DA and grow dorsally
252 between the somites and the notochord/neural tube. At 1.5 dpf, venous ISVs (vISVs)
253 sprout from the PCV, grow dorsally, and then with aISVs branch laterally to establish the
254 dorsal longitudinal anastomotic vessel (DLAV) that resides above the neural tube (Isogai

et al., 2003). By 2 dpf, the arterial and venous ISVs are mostly lumenized and reach from the DA/PCV below the notochord to the DLAV above the neural tube (Isogai et al., 2001).

Mural cells of the ISVs have been reported to emerge by either *de novo* differentiation of nearby mesenchyme followed by subsequent proliferation or through migration from the ventral side of the DA (Ando et al., 2016). Studies identifying the origin of ISV mural cells show that they are primarily derived from the sclerotome (Stratman et al., 2017, Rajan et al., 2020)—a sub-compartment of the somites and a derivative of paraxial mesoderm (Tani et al., 2020). Zebrafish have recently been shown to have a dorsal and ventral sclerotome, both of which contribute to the cells that associate with the ISVs: dorsal sclerotome populates the ISV region adjacent to the neural tube while ventral sclerotome populates the full ISV (Rajan et al., 2020, Ma et al., 2018). However, while the dorsal and ventral sclerotome cells can contribute to the development of different regions of the embryo (Ma et al., 2018), it is currently unclear whether they differ in gene expression.

Rajan et al recently described a population of sclerotome-derived cells called perivascular fibroblasts that associate with ISVs by 2 dpf and produce collagen matrix, thus providing structural support prior to mural cell migration or differentiation (Rajan et al., 2020). These cells are primarily derived from ventral sclerotome, are evenly distributed between arterial and venous ISVs, remain constant in number on the ISVs from 2 to 4 dpf, and express low levels of *pdgfrb* (Rajan et al., 2020). At 3 dpf, a subset—but not all—of perivascular fibroblasts will increase *pdgfrb* expression to become ISV mural cells (Rajan et al., 2020). Ando et al also describes a naïve *pdgfrb*-low mesenchymal population—likely the same cell type or similar to perivascular fibroblasts—that can mature into *pdgfrb*-high mural cells on the ISVs starting at approximately 2.5 dpf (Ando et al., 2016, Ando et al., 2021a).

Both studies observe that mural cells with *pdgfrb*-high expression are more apparent on aISVs than vISVs (Ando et al., 2016, Rajan et al., 2020), which is in part due to maturation of *pdgfrb*-low mesenchyme to *pdgfrb*-high mural cells through Notch signaling in arterial endothelium (Ando et al., 2019). Ando et al also observes that approximately 15% of mural cells are *tagln*-positive on ISVs by 5 dpf (Ando et al., 2019), potentially indicating further maturation of these *pdgfrb*-positive cells.

286 In support of these previous studies, we observed *pdgfrb*-low and -high cell
287 populations surrounding the ISVs up to 5 dpf in *Tg(tagln:NLS-EGFP); Tg(pdgfrb:Gal4FF;*
288 *UAS:RFP)* embryos (Figs 5A-H; S5A-I). Unexpectedly, we also detected *tagln*-low and -
289 high populations as early as 2 dpf (Figs 5C,D; S5A,B), prior to the developmental stages
290 in which ISV mural cells reportedly mature. While a subset of *tagln*-low cells in this region
291 were endothelial cells, we confirmed that many of the *tagln*-low and -high cells associated
292 with the early ISVs were perivascular (Fig. S4C,D), indicating that *tagln* may not
293 exclusively label mature mural cells, but instead also labels a subset of mural cell
294 precursors.

295 From our ISV data, we observed findings similar to that of the perivascular
296 fibroblasts (Rajan et al., 2020): the number of perivascular cells associated with the ISVs
297 remained constant between 2 to 5 dpf, the cells were equally distributed on aISVs and
298 vISVs, and *pdgfrb*-high cells became more apparent on aISVs than vISVs over time (Figs
299 5A-D; S5A-H). Furthermore, we were able to identify *pdgfrb*/*tagln* double-positive cells
300 with all combinations of high and low expression that increased in proportion up to 4 dpf
301 (Fig. 5E-G). Our data showed that double-positive cells were more common on aISVs
302 than vISVs and, as expected, the double-positive cells on the aISVs were more likely to
303 be *pdgfrb*-high (Fig. 5F,G). *tagln*-high mural cells were constant on all ISVs between 2-5
304 dpf (Fig. 5C,D), suggesting that on ISVs, mural cells may diverge from the typical
305 expression patterns of differentiation that would predict upregulated *tagln* at late stages
306 in the process of maturation.

307 *tagln*-low cells were the most common perivascular cell associated with the ISVs
308 at early timepoints (Fig. 5C,D). We speculated that the identity of these cells would
309 overlap with the previously described sclerotome-derived perivascular fibroblast
310 population. Indeed, when using the *twist1a* transgenic line as a sclerotome marker, we
311 identified *twist1a*-positive cells that reside at the notochord-neural tube interface and
312 notochord region as *tagln*-low, even prior to their association with the ISVs (Fig. S6A,D,E).
313 Conversely, a subset of cells that likely originated from the dorsal sclerotome—based on
314 their localization adjacent to the neural tube (Rajan et al., 2020)—were *tagln*-negative
315 (Fig. S6B,C). These data indicate that the ventral sclerotome is likely distinct from dorsal

316 sclerotome by the early and low expression of *tagln*. Additionally, these data reveal that
317 ISV mural cells can express *tagln* as precursors prior to upregulating *pdgfrb*.
318 We also observed consistent *tagln*/*pdgfrb* expression patterns in mural cells based
319 on their localization on the ISVs. *tagln* single-positive cells were more apparent on the
320 ISVs in the region adjacent to the notochord (Fig. 5H), consistent with previous reports of
321 ventral sclerotome migration to this region (Rajan et al., 2020, Ma et al., 2018). *pdgfrb*
322 single-positive cells were highly associated with the ISVs near to the neural tube (Fig.
323 5H), where the ISVs are primarily populated by dorsal sclerotome (Rajan et al., 2020).
324 Finally, *pdgfrb*/*tagln* double-positive cells were evident at two sites by 5 dpf—closest to
325 the notochord-neural tube interface (Fig. 5H), which could indicate a site-specific
326 maturation event, and near DA/aISV boundaries, which would suggest that these are
327 vSMCs from the ventral side of the DA that have migrated to the aISVs.
328
329 **A unique sclerotome-derived mural cell progenitor population resides along the**
330 **zebrafish midline**
331 From imaging *tagln*- and *pdgfrb*-positive cells near the ISVs in *Tg(tagln:NLS-*
332 *EGFP); Tg(pdgfrb:Gal4FF; UAS:RFP)* embryos, we discovered several cell populations
333 with unexpected *pdgfrb*/*tagln* expression near the midline. First, we note the medial floor
334 plate cells are *pdgfrb*/*tagln* double-positive (Fig. 6, MFP cells). Additionally, we observe
335 a *tagln* single-positive population of cells along the midline that accumulates below the
336 medial floor plate cells and above the notochord beginning at 3 dpf (Fig. 6, *tagln*+ midline
337 cells). Finally, we describe a mural cell progenitor population near the notochord-neural
338 tube interface that borders either side of the midline. This population—which begins as
339 *tagln* single-positive cells before acquiring *pdgfrb* expression—can be observed migrating
340 to the nearby ISVs from 2 to 5 dpf (Fig. 6, MC progenitor population).
341 Of the structures that reside at or near the midline, the medial floor plate is one of
342 the most recognizable due to its hourglass-like shape (Zheng et al., 2022). Medial floor
343 plate cells—which reside at the ventral side of the neural tube and contribute to neuronal
344 differentiation (Strähle et al., 2004)—have been previously identified as *pdgfrb*-positive
345 (Ando et al., 2016, Wiens et al., 2010). We observed intense *tagln* co-expression in the

346 medial floor plate cells from 1 to 5 dpf (Fig. 7A-K), indicating that *tagln* may have as-of-
347 yet unidentified developmental functions in primitive, non-muscular tissues.
348 Furthermore, we note a *tagln* single-positive population of elongated cells along
349 the midline beginning at 3 dpf that accumulates between the notochord and neural tube—
350 immediately ventral to the medial floor plate cells (Fig. 7A-K). This population appears to
351 organize as a continuous, thin, rod-like structure that is primarily one cell in width and
352 height. We confirmed that this *tagln*-positive midline cell population originates from the
353 sclerotome—unlike the adjacent medial floor plate—as evidenced by *twist1a* expression
354 (Fig. 7L-O). The function of this previously unidentified structure is currently unknown.
355 Finally, we observed a cell population—which we will term mural cell progenitors—
356 near the notochord-neural tube interface that borders either side of the midline and
357 migrates to the ISVs (Fig. 7A-W; Movies 2,3). At 1 dpf, these cells expressed *tagln*, but
358 not *pdgfrb* (Fig. 7A'), and at 2 dpf, a fraction of these cells began to express *pdgfrb* (Fig.
359 7C'). Over the next 3 days these cells elongated and increased *pdgfrb* expression until
360 approximately half were *pdgfrb*/*tagln* double-positive at 5 dpf (Fig. 7E',G',I').
361 Due to this mural cell progenitor population's proximity to the notochord and floor
362 plate, we questioned whether they originated from or resided within either of these
363 structures. Using a sonic hedgehog signaling molecule a (*shha*) transgenic line to label
364 the floor plate (Shkumatava et al., 2004, Ertzer et al., 2007), we were able to visualize the
365 mural cell progenitor population as sitting outside of the neural tube (Fig. S7A,B). Next,
366 we used a procollagen, type IX, alpha 2 (*col9a2*) transgenic line to visualize notochord
367 sheath cells in relation to the progenitor population (Garcia et al., 2017). Notochord
368 sheath cells are reported to express *tagln* in the notochord bud during regeneration
369 (Sinclair et al., 2021); therefore, we wanted to determine if the sheath cells may be the
370 source of the mural cell progenitor population. However, the progenitor population did not
371 overlap with notochord sheath cells (Fig. S7C,D), though we confirm that sheath cells do
372 express low levels of *tagln* during development (Fig. S7E). Jointly, these data showed
373 that the mural cell progenitor population abuts the neural tube and notochord, but does
374 not overlap with these structures.
375 We next used the sclerotome-marker *twist1a* and the neural crest-marker SRY-
376 box transcription factor 10 (*sox10*) transgenic lines (Lee et al., 2013, Kucenas et al., 2008)

377 to test the origins of this novel mural cell progenitor population. We identified this
378 progenitor population as exclusively derived from *twist1a*-positive sclerotome and not
379 *sox10*-positive neural crest (Figs 7L-O; S7F,G; Movie 3). Since Notch signaling from
380 arterial endothelium has been shown to be involved in maturation of mural cell progenitors
381 to *pdgfrb*-high mural cells (Ando et al., 2019), we speculated that the progenitor
382 population could be in contact with a blood vessel along the midline that would induce an
383 increase in *pdgfrb* expression. However, there is no blood vessel present along the
384 midline at this time point (Fig. S7H), nor do cells that increase *pdgfrb* expression in the
385 progenitor population reside near blood vessels (Fig. S7I,J). This suggests that the
386 induction of *pdgfrb* expression in this mural cell progenitor population is not controlled by
387 contact with the arterial vasculature.
388 Using *tagln*, *pdgfrb*, and *twist1a* as cellular markers, we observed cells from this
389 progenitor population migrate to the ISVs along the region adjacent to the notochord-
390 neural tube interface (Fig. 7P-W; Movies 2,3). Progenitor cells migrated to both aISVs
391 and vISVs from 2 to 5 dpf. Due to the location of this mural cell progenitor population in
392 relation to the ISVs, a proportion of the *pdgfrb*/*tagln* double-positive cells that we observe
393 on ISVs in the region closest to the notochord-neural tube interface (Fig. 5H) likely
394 originate from this progenitor source.
395
396 **Discussion:**
397 ***pdgfrb* and *tagln* transgenic zebrafish reporters**
398 In this study, we use *Tg(pdgfrb:Gal4FF; UAS:RFP)* and *Tg(tagln:NLS-EGFP)*
399 transgenic lines to identify single- and double-positive pericytes/vSMCs in the cranial,
400 axial, and ISVs at 1 to 5 dpf. Our nuclear-GFP *tagln* reporter facilitated identification of
401 novel *tagln*-positive cells in the zebrafish trunk. High *tagln* expression is evident in skeletal
402 muscle, which has made it difficult in the past to explore *tagln* expression patterns in cells
403 near to the skeletal muscle with cytosolic-GFP *tagln* reporters. With the nuclear-GFP *tagln*
404 reporter, we have revealed *tagln* expression in the hypochord, the medial floor plate, and
405 in sclerotome-derived mesenchyme in the trunk region.
406 To rule out whether these expression patterns were an artifact of the nuclear-GFP
407 *tagln* reporter, we sought to confirm *tagln* expression in these structures using an

408 independently generated cytosolic-GFP *tagln* reporter (*Tg(tagln:EGFP)*; Fig. S8A-H). As
409 expected, GFP expression in the skeletal muscle decreased the efficiency and resolution
410 of identifying *tagln*-positive cells in the trunk, though we were able to visualize GFP
411 expression in the hypochord, ISV mural cells, the novel mural cell progenitor population
412 we describe, the medial floor plate, and *tagln*-positive midline cells. Thus, despite high
413 background GFP signal, we validate *tagln* expression in these structures using the
414 cytosolic-GFP *tagln* reporter.

415 The *pdgfrb* reporter line—which utilizes the Gal4/UAS system (Ando et al., 2016)—
416 presented with occasional RFP expression mosaicism. This mosaicism, when present,
417 was most apparent in the medial floor plate cells (Fig. 7A-J), though it is difficult to assess
418 the penetrance at which other structures were affected. Due to this, there may be *pdgfrb*-
419 positive cells that are underrepresented in this study, particularly cells that express low
420 levels of *pdgfrb*. However, despite potential mosaicism issues, the expression patterns
421 that we visualized over time and in various regions were consistent across all samples.
422

423 **Cranial Mural Cells**

424 Previous reports show that *pdgfrb*-positive pericytes are the predominant mural
425 cell in the mid- and hindbrain prior to 5 dpf, at which point arterial-associated mural cells
426 begin to express *tagln* and other vSMC markers (Ando et al., 2019, Ando et al., 2016,
427 Ando et al., 2021a, Whitesell et al., 2014, Wang et al., 2014). We observed similar
428 findings, in that *pdgfrb* single-positive pericytes were the most prevalent type of mural cell
429 along embryonic cranial vessels, with eventual *tagln* co-expression evident—yet sparsely
430 represented—in a subset of *pdgfrb*-positive arterial mural cells at 4 dpf. No *tagln* single-
431 positive cells were detected at the time points assessed. Based on these data, and
432 supported by the findings of previous studies, we conclude that *pdgfrb* is an ideal reporter
433 to visualize cranial mural cell association with blood vessels up to 5 dpf, with the caveat
434 that a large proportion of early *pdgfrb*-positive cranial cells are neural crest or
435 mesenchyme progenitors that are not associated with vessels.
436

437 **Mural Cells of the Axial Vessels**

438 In the axial vessels (i.e. DA, PCV, CA, and CV), we corroborate the previous
439 findings regarding vSMC expression patterns on the ventral side of the DA (Ando et al.,
440 2021a, Stratman et al., 2017, Ando et al., 2016, Ando et al., 2019). Specifically, we detect
441 *pdgfrb* single-positive cells at 2 dpf, where they then expand in number and increase
442 expression of *tagln* starting at 3 dpf (Fig. 2). Moreover, we observe a slow and sporadic
443 increase of *pdgfrb* single-positive cells on the PCV between 1 to 5 dpf (Fig. 2). At 5 dpf,
444 there are twice as many *pdgfrb*-positive mural cells associated with the ventral side of the
445 DA than the entire PCV, which highlights the clear difference in the magnitude of mural
446 cell recruitment between arteries and veins early in development.
447 Our analysis of both the anterior and caudal axial vessels also reveals that
448 accumulation and maturation of these mural cells occurs in an anterior to posterior
449 fashion. By 1 dpf, the anterior and posterior regions of the main axial vessels have formed,
450 somite segmentation has been completed, and the sclerotome is distinct from other
451 somitic tissues (Stickney et al., 2000). Despite this, DA vSMCs—which are mainly derived
452 from the sclerotome (Stratman et al., 2017)—mature one to two days earlier than the
453 vSMCs of the CA (Fig. 2). There may be several reasons for this delay, with one
454 hypothesis being that the DA provides earlier signals than the CA to initiate maturation of
455 vSMCs. Alternatively, since somites develop in an anterior to posterior wave (Stickney et
456 al., 2000), the age of the somites from which mural cells are derived could influence the
457 timing of vSMC maturation, even after vSMCs have accumulated on the vessels. More
458 work will be needed in this area to resolve the cues driving this temporal differentiation
459 pattern.
460
461 **The Hypochord as a Source of *tagln*-Positive Cells**
462 Through use of the nuclear-GFP *tagln* reporter, we found that the hypochord
463 contributes to *tagln*-positive cells along the dorsal side of the DA up to at least 5 dpf (Fig.
464 2). Interestingly, the hypochord and medial floor plate—which we also show is *tagln*-
465 positive—are among the earliest structures in the zebrafish embryo to co-express *pdgfrb*
466 and *tagln*. The hypochord, floor plate, and notochord have been shown to be derived from
467 the multipotent midline progenitor cells in the dorsal organizer or the tailbud (Row et al.,
468 2016, Latimer and Appel, 2006)—a common origin which may, in part, explain how two

469 structures that are dissimilar in function share this unique expression pattern.
470 Furthermore, in the invertebrate *Ciona*, researchers show that a series of
471 calponin/transgelin family genes (*tagln-r.b, tagln-r.c, tagln-r.d, tagln-r.e*) are expressed in
472 the *Ciona* floor plate, notochord, and endodermal strand (the *Ciona* analogue for the
473 hypochord), indicating that Tagln expression in midline structures may have a conserved
474 role in embryogenesis (Oonuma et al., 2021). As Tagln is known primarily as an actin-
475 binding protein in contractile cells, the role of Tagln in these non-contractile, non-
476 muscular, primitive midline structures remains unknown.

477 The persistence of the elongated *tagln*-positive cells on the dorsal side of the DA
478 indicates that the cells of the hypochord are not entirely transient, as previously assumed.
479 While previous studies have observed hypochord cells undergoing apoptosis (Löfberg
480 and Collazo, 1997, Cleaver et al., 2000), we propose that a subset of hypochord cells
481 survive and reprogram their cellular function and morphology after the DA has been
482 appropriately oriented. Due to the maintained expression of *tagln* and proximity to the DA,
483 we propose these cells may undertake a mural cell role; however, further research is
484 needed to determine whether these cells function similarly to other vSMC populations.

485 As the hypochord is present exclusively in fish and amphibians, we questioned
486 whether there is an analogous mammalian structure that could contribute to Tagln-
487 positive cells on the DA of amniotes. Previous reports speculate that the dorsal
488 endoderm—a midline structure that originates from the midline precursor cell population
489 and forms ventral to the notochord (Peyrot et al., 2011)—may play a role in angioblast
490 and DA formation (Poole et al., 2001), similar to the hypochord. However, while the
491 endoderm gives rise to the intestines, lung, liver, and other organs (Wlizla and Zorn,
492 2015), there are no known reports of endoderm contributing to mural cell populations in
493 amniotes (Holm et al., 2018).

494 In the mouse embryo, the dorsal and ventral sides of the DA are populated by
495 vSMCs from different sources: the ventral side is first populated by cells from the lateral
496 plate mesoderm, with dorsal vSMCs originating from the somites. Over time, the vSMCs
497 from the lateral plate mesoderm disappear, and the ventral side then becomes populated
498 with somitic vSMCs (Wasteson et al., 2008). While this process is not identical on the
499 zebrafish DA—given that somitic vSMCs are the initial populators of the ventral side of

500 the DA in zebrafish—it does indicate that dorsal and ventral vSMCs can arise from
501 divergent origins and supports that this could be a conserved process.
502
503 **Mural Cells of the Intersegmental Vessels**
504 In the ISV region, we note perivascular cells associated with the vessels exhibiting
505 all combinations of high and low expression of *pdgfrb* and *tagln*. To summarize, *pdgfrb*-
506 high cells were more common on arterial than venous ISVs and increased in number over
507 time. *pdgfrb*/*tagln* double-positive cells were also more common on aISVs and were more
508 likely to be *pdgfrb*-high on aISVs than vISVs. *tagln*-high cells were constant in number
509 between 2 to 5 dpf, and *tagln*-low cells—the most common expression pattern
510 represented—were revealed to be sclerotome-derived cells that were migrating to or
511 associated with the ISVs. Further, expression patterns were related to mural cell location
512 on the ISVs, with *pdgfrb* single-positive cells more likely to be found on the dorsal ISV
513 region, double-positive cells nearest to the notochord-neural tube interface, and *tagln*
514 single-positive cells primarily near the notochord ISV region by 5 dpf (Fig. 5H).
515 These data indicate that *tagln* may not exclusively label mature mural cells, but
516 instead could also label a subset of mural cell precursors in the trunk. These precursors
517 likely overlap with the perivascular fibroblast population described by Rajan et al (Rajan
518 et al., 2020), as they are both sclerotome-derived and populate the ISVs prior to reported
519 mural cell maturation. This would suggest that a subset, but not all, of the *tagln*-positive
520 early precursors on the ISVs will mature into mural cells.
521
522 **Sclerotome-Derived *tagln*-Positive Cell Populations in the Trunk**
523 Use of our nuclear-GFP *tagln* reporter allowed us to ascertain that sclerotome-
524 derived cells in the zebrafish trunk are primarily *tagln*-positive as early as 1 dpf. Due to
525 the main localization of these *tagln*-positive cells at the notochord-neural tube interface
526 or below, we speculate that the *twist1a*/*tagln* double-positive cells arise from the ventral
527 sclerotome, with *twist1a*-positive/*tagln*-negative cells descending from the dorsal
528 sclerotome. Of note, there are two unique sites where sclerotome-derived *tagln*-positive
529 cells accumulate during development.

First, we identified a *twist1a*/*tagln* double-positive midline population between the neural tube and notochord. This population begins to accumulate beneath the medial floor plate cells at 3 dpf and exhibits high *tagln* expression (Fig. 6, *tagln*+ midline cells). Though this structure's function is unknown, its location would suggest that it may exist as a cushion or as structural support to the notochord-neural tube interface.

Second, we identified a mural cell progenitor population that resides adjacent to the midline at the notochord-neural tube interface. This *tagln*-positive population upregulates *pdgfrb* expression sporadically in an increasing number of cells between 2 to 5 dpf and migrates to the ISVs (Fig. 6, MC progenitor population; Movies 2,3). Due to the location of this mural cell progenitor population in relation to the ISVs, we suspect that a proportion of the *pdgfrb*/*tagln* double-positive cells that we observe on ISVs in the region closest to the notochord-neural tube interface likely originate from this progenitor source. Uniquely, the upregulation of *pdgfrb* expression in this mural cell progenitor population occurs independently of contact with arterial endothelium. We hypothesize that upregulation of *pdgfrb* confers motility cues to the mural cell progenitors to then migrate to blood vessels; however, further studies are needed to determine the mechanisms behind this seemingly stochastic *pdgfrb* upregulation.

This progenitor population also demonstrates that mural cell precursors can express *tagln* prior to upregulating *pdgfrb*. Since *pdgfrb* is associated with precursor populations and *tagln* is regarded as a mature vSMC marker, this finding suggests that the expression patterns related to mural cell maturation are more nuanced than previously reported. Therefore, we ask: what role could Tagln play prior to Pdgfrb upregulation? Several studies report that Tagln assists in cell motility: loss of Tagln decreases motility (Elsafadi et al., 2016), whereas overexpression leads to pathological motility in situations such as metastatic cancer (Zhou et al., 2016, Chen et al., 2019). Since sclerotome cells are inherently migratory as they populate and form various tissues, this could help explain the early expression of Tagln in mural cell precursors during embryogenesis. Future work in this area will continue to reveal exciting new findings driving site-specific and temporal regulation of mural cell biology.

561 **Materials and Methods:**

562 **Zebrafish**

563 Zebrafish (*Danio rerio*) embryos were raised and maintained as described (Westerfield,
564 2000, Kimmel et al., 1995). Zebrafish husbandry and research protocols were reviewed
565 and approved by the WUSTL Animal Care and Use Committee. Established transgenic
566 lines that were used in this study are listed in the table below.

567

Genotype	Allele	Origin
Tg(-2.4shha-ABC:GFP)	*sb15*	(Shkumatava et al., 2004)
Tg(col9a2:mCherry)	*pd1150*	(Garcia et al., 2017)
Tg(kdrl:mCherry-CAAX)	*y171*	(Fujita et al., 2011)
Tg(Ola.Twist:GAL4)	*sq11*	(Lee et al., 2013)
Tg(sox10:mRFP)	*vu234*	(Kucenas et al., 2008)
Tg(tagln:eGFP)	*p151*	(Seiler et al., 2010)
Tg(tagln:NLS-EGFP-2A-CFP-FTASE)	*y450*	(Stratman et al., 2017)
Tg(5xUAS:RFP)	*zf83*	(Asakawa et al., 2008)
TgBAC(pdgfrb:Gal4FF)	*ncv24*	(Ando et al., 2016)

568

569 **Image Acquisition and Processing**

570 Embryos and larvae were anesthetized in buffered 0.2 mg/mL Tricaine-S (Western
571 Chemical, Inc; NC0872873) and mounted in 0.8% low-melting point agarose (IBI
572 Scientific; #IB70056) on a 35-mm glass-bottom petri dish (MatTek; #P35G-1.5-20-C).
573 Confocal images were obtained using a 4x or 40x objective with a W1 Spinning Disk
574 confocal microscope, a Fusion camera, and the Nikon Eclipse Ti2-E base. Images were
575 then deconvolved using Nikon's NIS-Elements software. Fiji image processing software
576 was used for counting number of cells per vessel length and for generating final images.
577 Embryos were consistently imaged in the afternoon hours, thus: '1 dpf' represents
578 embryos between 28-34 hours post-fertilization (hpf); '2 dpf' represents 52-58 hpf; '3 dpf'
579 represents 76-82 hpf; '4 dpf' represents 100-106 hpf; '5 dpf' represents 124-130 hpf. At
580 least 6 embryos were imaged and analyzed per developmental timepoint.

581

Acknowledgements:

We thank Tony Tsai's lab for the *Tg(-2.4shha-ABC:GFP)* line, Shawn Burgess's lab for the *Tg(col9a2:mCherry)* line, and Mayssa Mokalled's lab for the *Tg(sox10:mRFP)* line. Figure schematics were generated using BioRender.com.

Competing Interests:

The authors declare that they have no conflicts of interest.

Funding:

This work was supported by grants from the NIH/NIGMS R35 GM137976 (A.N.S.); Children's Discovery Institute of Washington University and St. Louis Children's Hospital (A.N.S.); the Washington University Institute of Clinical and Translational Sciences which is, in part, supported by the NIH/National Center for Advancing Translational Sciences (NCATS), CTSA grant #UL1TR002345 (A.N.S.); and American Heart Association Postdoctoral Fellowship Award #906436 (S.C.).

598 **References:**

599

600 Ando, K., Fukuhara, S., Izumi, N., Nakajima, H., Fukui, H., Kelsh, R. N. & Mochizuki, N.
601 (2016). Clarification of mural cell coverage of vascular endothelial cells by live
602 imaging of zebrafish. *Development,* 143**,** 1328-1339. 10.1242/dev.132654

603 Ando, K., Ishii, T. & Fukuhara, S. (2021a). Zebrafish Vascular Mural Cell Biology: Recent
604 Advances, Development, and Functions. *Life (Basel),* 11. 10.3390/life11101041

605 Ando, K., Shih, Y.-H., Ebarasi, L., Grosse, A., Portman, D., Chiba, A., Mattonet, K., Gerri,
606 C., Stainier, D. Y. R., Mochizuki, N., Fukuhara, S., Betsholtz, C. & Lawson, N. D.
607 (2021b). Conserved and context-dependent roles for pdgfrb signaling during
608 zebrafish vascular mural cell development. *Developmental Biology,* 479**,** 11-22.
609 https://doi.org/10.1016/j.ydbio.2021.06.010

610 Ando, K., Wang, W., Peng, D., Chiba, A., Lagendijk, A. K., Barske, L., Crump, J. G.,
611 Stainier, D. Y. R., Lendahl, U., Koltowska, K., Hogan, B. M., Fukuhara, S.,
612 Mochizuki, N. & Betsholtz, C. (2019). Peri-arterial specification of vascular mural
613 cells from naïve mesenchyme requires Notch signaling. *Development,* 146.
614 10.1242/dev.165589

615 Armulik, A., Abramsson, A. & Betsholtz, C. (2005). Endothelial/Pericyte Interactions.
616 *Circulation Research,* 97**,** 512-523. doi:10.1161/01.RES.0000182903.16652.d7

617 Asakawa, K., Suster, M. L., Mizusawa, K., Nagayoshi, S., Kotani, T., Urasaki, A.,
618 Kishimoto, Y., Hibi, M. & Kawakami, K. (2008). Genetic dissection of neural circuits
619 by Tol2 transposon-mediated Gal4 gene and enhancer trapping in
620 zebrafish. *Proceedings of the National Academy of Sciences,* 105**,** 1255-1260.
621 doi:10.1073/pnas.0704963105

622 Chakraborty, R., Saddouk, F. Z., Carrao, A. C., Krause, D. S., Greif, D. M. & Martin, K. A.
623 (2019). Promoters to Study Vascular Smooth Muscle. *Arteriosclerosis,*
624 *Thrombosis, and Vascular Biology,* 39**,** 603-612.
625 doi:10.1161/ATVBAHA.119.312449

626 Chen, Z., He, S., Zhan, Y., He, A., Fang, D., Gong, Y., Li, X. & Zhou, L. (2019). TGF-b-
627 induced transgelin promotes bladder cancer metastasis by regulating epithelial-
628 mesenchymal transition and invadopodia formation. *eBioMedicine,* 47**,** 208-220.
629 10.1016/j.ebiom.2019.08.012

630 Cleaver, O., Seufert, D. W. & Krieg, P. A. (2000). Endoderm patterning by the notochord:
631 development of the hypochord in Xenopus. *Development,* 127**,** 869-879.
632 10.1242/dev.127.4.869

633 Donadon, M. & Santoro, M. M. (2021). The origin and mechanisms of smooth muscle cell
634 development in vertebrates. *Development,* 148. 10.1242/dev.197384

635 Elsafadi, M., Manikandan, M., Dawud, R. A., Alajez, N. M., Hamam, R., Alfayez, M.,
636 Kassem, M., Aldahmash, A. & Mahmood, A. (2016). Transgelin is a TGFβ-
637 inducible gene that regulates osteoblastic and adipogenic differentiation of human
638 skeletal stem cells through actin cytoskeleston organization. *Cell Death Dis,* 7**,**
639 e2321. 10.1038/cddis.2016.196

640 Eriksson, J. & Löfberg, J. (2000). Development of the hypochord and dorsal aorta in the
641 zebrafish embryo (Danio rerio). *Journal of Morphology,* 244**,** 167-176.
642 https://doi.org/10.1002/(SICI)1097-4687(200006)244:3<167::AID-
643 JMOR2>3.0.CO;2-J

644 Ertzer, R., Müller, F., Hadzhiev, Y., Rathnam, S., Fischer, N., Rastegar, S. & Strähle, U.
645 (2007). Cooperation of sonic hedgehog enhancers in midline expression.
646 *Developmental Biology,* 301**,** 578-589. https://doi.org/10.1016/j.ydbio.2006.11.004

647 Fujita, M., Cha, Y. R., Pham, V. N., Sakurai, A., Roman, B. L., Gutkind, J. S. & Weinstein,
648 B. M. (2011). Assembly and patterning of the vascular network of the vertebrate
649 hindbrain. *Development,* 138**,** 1705-1715. 10.1242/dev.058776

650 Garcia, J., Bagwell, J., Njaine, B., Norman, J., Levic, D. S., Wopat, S., Miller, S. E., Liu,
651 X., Locasale, J. W., Stainier, D. Y. R. & Bagnat, M. (2017). Sheath Cell Invasion
652 and Trans-differentiation Repair Mechanical Damage Caused by Loss of Caveolae
653 in the Zebrafish Notochord. *Current Biology,* 27**,** 1982-1989.e3.
654 https://doi.org/10.1016/j.cub.2017.05.035

655 Hellstrom, M., Kal N, M., Lindahl, P., Abramsson, A. & Betsholtz, C. (1999). Role of
656 PDGF-B and PDGFR-beta in recruitment of vascular smooth muscle cells and
657 pericytes during embryonic blood vessel formation in the mouse. *Development,*
658 126**,** 3047-3055.

659 Holm, A., Heumann, T. & Augustin, H. G. (2018). Microvascular Mural Cell Organotypic
660 Heterogeneity and Functional Plasticity. *Trends in Cell Biology,* 28**,** 302-316.
661 10.1016/j.tcb.2017.12.002

662 Isogai, S., Horiguchi, M. & Weinstein, B. M. (2001). The Vascular Anatomy of the
663 Developing Zebrafish: An Atlas of Embryonic and Early Larval Development.
664 *Developmental Biology,* 230**,** 278-301. https://doi.org/10.1006/dbio.2000.9995

665 Isogai, S., Lawson, N. D., Torrealday, S., Horiguchi, M. & Weinstein, B. M. (2003).
666 Angiogenic network formation in the developing vertebrate trunk. *Development,*
667 130**,** 5281-5290. 10.1242/dev.00733

668 Kimmel, C. B., Ballard, W. W., Kimmel, S. R., Ullmann, B. & Schilling, T. F. (1995). Stages
669 of embryonic development of the zebrafish. *Dev Dyn,* 203**,** 253-310.
670 10.1002/aja.1002030302

671 Kucenas, S., Takada, N., Park, H.-C., Woodruff, E., Broadie, K. & Appel, B. (2008). CNS-
672 derived glia ensheath peripheral nerves and mediate motor root development.
673 *Nature Neuroscience,* 11**,** 143-151. 10.1038/nn2025

674 Latimer, A. J. & Appel, B. (2006). Notch signaling regulates midline cell specification and
675 proliferation in zebrafish. *Developmental Biology,* 298**,** 392-402.
676 https://doi.org/10.1016/j.ydbio.2006.05.039

677 Lee, R. T. H., Knapik, E. W., Thiery, J. P. & Carney, T. J. (2013). An exclusively
678 mesodermal origin of fin mesenchyme demonstrates that zebrafish trunk neural
679 crest does not generate ectomesenchyme. *Development,* 140**,** 2923-2932.
680 10.1242/dev.093534

681 Leonard, E. V., Figueroa, R. J., Bussmann, J., Lawson, N. D., Amigo, J. D. & Siekmann,
682 A. F. (2022). Regenerating vascular mural cells in zebrafish fin blood vessels are
683 not derived from pre-existing mural cells and differentially require Pdgfrb signalling
684 for their development. *Development,* 149. 10.1242/dev.199640

685 Li, L., Miano, J. M., Cserjesi, P. & Olson, E. N. (1996). SM22α, a Marker of Adult Smooth
686 Muscle, Is Expressed in Multiple Myogenic Lineages During Embryogenesis.
687 *Circulation Research,* 78**,** 188-195. doi:10.1161/01.RES.78.2.188

688 Löfberg, J. & Collazo, A. (1997). Hypochord, an enigmatic embryonic structure: Study of
689 the axolotl embryo. *Journal of Morphology,* 232**,** 57-66.
690 https://doi.org/10.1002/(SICI)1097-4687(199704)232:1<57::AID-
691 JMOR3>3.0.CO;2-L

692 Ma, R. C., Jacobs, C. T., Sharma, P., Kocha, K. M. & Huang, P. (2018). Stereotypic
693 generation of axial tenocytes from bipartite sclerotome domains in zebrafish. *PLoS*
694 *Genet,* 14**,** e1007775. 10.1371/journal.pgen.1007775

695 Majesky, M. W. (2007). Developmental Basis of Vascular Smooth Muscle Diversity.
696 *Arteriosclerosis, Thrombosis, and Vascular Biology,* 27**,** 1248-1258.
697 doi:10.1161/ATVBAHA.107.141069

698 Oonuma, K., Yamamoto, M., Moritsugu, N., Okawa, N., Mukai, M., Sotani, M., Tsunemi,
699 S., Sugimoto, H., Nakagome, E., Hasegawa, Y., Shimai, K., Horie, T. & Kusakabe,
700 T. G. (2021). Evolution of Developmental Programs for the Midline Structures in
701 Chordates: Insights From Gene Regulation in the Floor Plate and Hypochord
702 Homologues of Ciona Embryos. *Front Cell Dev Biol,* 9**,** 704367.
703 10.3389/fcell.2021.704367

704 Owens, G. K., Kumar, M. S. & Wamhoff, B. R. (2004). Molecular Regulation of Vascular
705 Smooth Muscle Cell Differentiation in Development and Disease. *Physiological*
706 *Reviews,* 84**,** 767-801. 10.1152/physrev.00041.2003

707 Peyrot, S. M., Wallingford, J. B. & Harland, R. M. (2011). A revised model of Xenopus
708 dorsal midline development: Differential and separable requirements for Notch and

Shh signaling. *Developmental Biology,* 352**,** 254-266. https://doi.org/10.1016/j.ydbio.2011.01.021

Poole, T. J., Finkelstein, E. B. & Cox, C. M. (2001). The role of FGF and VEGF in angioblast induction and migration during vascular development. *Developmental Dynamics,* 220**,** 1-17. https://doi.org/10.1002/1097-0177(2000)9999:9999<::AID-DVDY1087>3.0.CO;2-2

Rajan, A. M., Ma, R. C., Kocha, K. M., Zhang, D. J. & Huang, P. (2020). Dual function of perivascular fibroblasts in vascular stabilization in zebrafish. *PLOS Genetics,* 16**,** e1008800. 10.1371/journal.pgen.1008800

Rensen, S. S., Doevendans, P. A. & Van Eys, G. J. (2007). Regulation and characteristics of vascular smooth muscle cell phenotypic diversity. *Neth Heart J,* 15**,** 100-8. 10.1007/bf03085963

Row, R. H., Tsotras, S. R., Goto, H. & Martin, B. L. (2016). The zebrafish tailbud contains two independent populations of midline progenitor cells that maintain long-term germ layer plasticity and differentiate in response to local signaling cues. *Development,* 143**,** 244-54. 10.1242/dev.129015

Santoro, M. M., Pesce, G. & Stainier, D. Y. (2009). Characterization of vascular mural cells during zebrafish development. *Mech Dev,* 126**,** 638-49. 10.1016/j.mod.2009.06.1080

Seiler, C., Abrams, J. & Pack, M. (2010). Characterization of zebrafish intestinal smooth muscle development using a novel sm22α-b promoter. *Developmental Dynamics,* 239**,** 2806-2812. https://doi.org/10.1002/dvdy.22420

Shih, Y.-H., Portman, D., Idrizi, F., Grosse, A. & Lawson, N. D. (2021). Integrated molecular analysis identifies a conserved pericyte gene signature in zebrafish. *Development,* 148. 10.1242/dev.200189

Shkumatava, A., Fischer, S., MüLler, F., Strahle, U. & Neumann, C. J. (2004). Sonic hedgehog, secreted by amacrine cells, acts as a short-range signal to direct differentiation and lamination in the zebrafish retina. *Development,* 131**,** 3849-3858. 10.1242/dev.01247

Sinclair, J. W., Hoying, D. R., Bresciani, E., Nogare, D. D., Needle, C. D., Berger, A., Wu, W., Bishop, K., Elkahloun, A. G., Chitnis, A., Liu, P. & Burgess, S. M. (2021). The Warburg effect is necessary to promote glycosylation in the blastema during zebrafish tail regeneration. *NPJ Regen Med,* 6**,** 55. 10.1038/s41536-021-00163-x

Smith, C. L. & Tallquist, M. D. (2010). PDGF function in diverse neural crest cell populations. *Cell Adh Migr,* 4**,** 561-6. 10.4161/cam.4.4.12829

744 Stickney, H. L., Barresi, M. J. F. & Devoto, S. H. (2000). Somite development in zebrafish.
745 *Developmental Dynamics,* 219**,** 287-303. https://doi.org/10.1002/1097-
746 0177(2000)9999:9999<::AID-DVDY1065>3.0.CO;2-A

747 Strähle, U., Lam, C. S., Ertzer, R. & Rastegar, S. (2004). Vertebrate floor-plate
748 specification: variations on common themes. *Trends in Genetics,* 20**,** 155-162.
749 https://doi.org/10.1016/j.tig.2004.01.002

750 Stratman, A. N., Burns, M. C., Farrelly, O. M., Davis, A. E., Li, W., Pham, V. N.,
751 Castranova, D., Yano, J. J., Goddard, L. M., Nguyen, O., Galanternik, M. V., Bolan,
752 T. J., Kahn, M. L., Mukouyama, Y. S. & Weinstein, B. M. (2020). Chemokine
753 mediated signalling within arteries promotes vascular smooth muscle cell
754 recruitment. *Commun Biol,* 3**,** 734. 10.1038/s42003-020-01462-7

755 Stratman, A. N., Pezoa, S. A., Farrelly, O. M., Castranova, D., Dye, L. E., Butler, M. G.,
756 Sidik, H., Talbot, W. S. & Weinstein, B. M. (2017). Interactions between mural cells
757 and endothelial cells stabilize the developing zebrafish dorsal aorta. *Development,*
758 144**,** 115-127. 10.1242/dev.143131

759 Tani, S., Chung, U.-I., Ohba, S. & Hojo, H. (2020). Understanding paraxial mesoderm
760 development and sclerotome specification for skeletal repair. *Experimental &*
761 *Molecular Medicine,* 52**,** 1166-1177. 10.1038/s12276-020-0482-1

762 Tsuji-Tamura, K., Morino-Koga, S., Suzuki, S. & Ogawa, M. (2021). The canonical smooth
763 muscle cell marker TAGLN is present in endothelial cells and is involved in
764 angiogenesis. *Journal of Cell Science,* 134. 10.1242/jcs.254920

765 Ulrich, F., Ma, L.-H., Baker, R. G. & Torres-Vázquez, J. (2011). Neurovascular
766 development in the embryonic zebrafish hindbrain. *Developmental Biology,* 357**,**
767 134-151. https://doi.org/10.1016/j.ydbio.2011.06.037

768 Wang, Y., Pan, L., Moens, C. B. & Appel, B. (2014). Notch3 establishes brain vascular
769 integrity by regulating pericyte number. *Development,* 141**,** 307-317.
770 10.1242/dev.096107

771 Wasteson, P., Johansson, B. R., Jukkola, T., Breuer, S., AkyüRek, L. M., Partanen, J. &
772 Lindahl, P. (2008). Developmental origin of smooth muscle cells in the descending
773 aorta in mice. *Development,* 135**,** 1823-1832. 10.1242/dev.020958

774 Westerfield, M. (2000). *The zebrafish book. A guide for the laboratory use of zebrafish*
775 *(Danio rerio),* Eugene, Univ. of Oregon Press.

776 Whitesell, T. R., Kennedy, R. M., Carter, A. D., Rollins, E. L., Georgijevic, S., Santoro, M.
777 M. & Childs, S. J. (2014). An α-smooth muscle actin (acta2/αsma) zebrafish
778 transgenic line marking vascular mural cells and visceral smooth muscle cells.
779 *PLoS One,* 9**,** e90590. 10.1371/journal.pone.0090590

780 Wiens, K. M., Lee, H. L., Shimada, H., Metcalf, A. E., Chao, M. Y. & Lien, C.-L. (2010).
781 Platelet-Derived Growth Factor Receptor β Is Critical for Zebrafish Intersegmental
782 Vessel Formation. *PLOS ONE,* 5**,** e11324. 10.1371/journal.pone.0011324

783 Wlizla, M. & Zorn, A. M. (2015). Chapter 13 - Vertebrate Endoderm Formation. *In:* Moody,
784 S. A. (ed.) *Principles of Developmental Genetics (Second Edition).* Oxford:
785 Academic Press.

786 Zheng, P., Xie, H., Zhu, P. & Zhao, C. (2022). Distribution and characteristics of neurons
787 at the nerve base plate of zebrafish. *Heredity,* 44**,** 510-520. 10.16288/j.yczz.22-
788 074

789 Zhou, H.-M., Fang, Y.-Y., Weinberger, P. M., Ding, L.-L., Cowell, J. K., Hudson, F. Z.,
790 Ren, M., Lee, J. R., Chen, Q.-K., Su, H., Dynan, W. S. & Lin, Y. (2016). Transgelin
791 increases metastatic potential of colorectal cancer cells in vivo and alters
792 expression of genes involved in cell motility. *BMC Cancer,* 16**,** 55.
793 10.1186/s12885-016-2105-8
794

795

796

797 **Figure Legends:**

798

799 **Figure 1: Coronal views of *Tg(tagln:NLS-EGFP); Tg(pdgfrb:Gal4FF; UAS:RFP)***
800 **zebrafish brains from 1 to 5 dpf.** (A) Schematic diagram illustrating the orientation for
801 imaging brain coronal sections: the lower middle region (yellow) and upper middle region
802 (purple). (B-J) Maximum intensity projection images of the mid- and hindbrain from 1 to 5
803 dpf. (B'-J') Outlines of the blood vessels visualized in the confocal images; pink
804 represents arteries and blue represents veins. At 1 dpf (B) *pdgfrb*-positive cells are
805 associated with the PHBC. At 2 dpf (C,D) *pdgfrb*-positive cells begin to accumulate
806 around the CoW (C, comprised of the BCA and PCS) and on the CtAs (D). *pdgfrb*-positive
807 cells continue to accumulate on the CoW and CtAs from 3 to 5 dpf (E-J). A single
808 *pdgfrb*/*tagln* double-positive cell is evident on the MMCtA at 4 dpf (H, inset). Schematic
809 created with BioRender.com. AMCtA, anterior mesencephalic central artery. BA, basilar
810 artery. BCA, basal communicating artery. CaDI, caudal division of the internal carotid
811 artery. CCtA, cerebellar central artery. CoW, Circle of Willis. MMCtA, middle
812 mesencephalic central artery. MtA, metencephalic artery. PCS, posterior communicating
813 segment. PHBC, primordial hindbrain channel. PMCtA, posterior mesencephalic central
814 artery. Scale bars: 50 µm.

815

816 **Figure 2: Summary of mural cell accumulation on the axial vasculature.** The
817 hypochord—which begins as a *pdgfrb*/*tagln* double-positive structure—is a novel source
818 of *tagln*-positive cells on the dorsal side of the dorsal aorta and caudal artery. At 2 dpf,
819 the hypochord cells began to delaminate on the dorsal aorta. At 3 dpf, the *pdgfrb*/*tagln*
820 double-positive cells begin to decrease *pdgfrb* expression. By 4 dpf, these cells were *tagln*
821 single-positive. In the caudal region, this hypochord reprogramming event began 1 day
822 later than the anterior region. On the ventral side of the dorsal aorta and caudal vein,
823 *pdgfrb* single-positive vSMCs were observed beginning at 2 dpf, where they then
824 expanded in number and increased expression of *tagln*. By 5 dpf, *pdgfrb*/*tagln* double-
825 positive cells accounted for approximately 60% of ventral vSMCs on the dorsal aorta, and
826 no *tagln* single-positive cells were detected. The vSMCs on the ventral side of the CA
827 accumulated more slowly and did not begin co-expressing *tagln* until 5 dpf, which

amounted to a 2-day delay compared to the anterior region. Finally, we observed a slow accumulation of *pdgfrb* single-positive cells on the posterior cardinal vein and caudal vein between 1 to 5 dpf. *tagln*-positive cells were particularly sparse on the veins, but visible at later stages.

Figure 3: *tagln* and *pdgfrb* expression along the dorsal aorta and cardinal vein of 1 to 5 dpf *Tg(tagln:NLS-EGFP); Tg(pdgfrb:Gal4FF; UAS:RFP)* zebrafish. (A-E) Maximum intensity projection images of the DA and PCV from 1 to 5 dpf. (A'-E') The images from A-E without the brightfield overlay. (F-G) Bar and line graph representations of the number of single- and double-positive cells on the dorsal side of the DA (F), the ventral side of the DA (G), and the PCV (H). (I) Schematic diagram illustrating the imaged region. Schematic created with BioRender.com. At least 6 embryos were analyzed at each age. DA, dorsal aorta. PCV, posterior cardinal vein. HC, hypochord. NC, notochord. Scale bars: 50 µm.

Figure 4: *tagln* and *pdgfrb* expression along the caudal artery and vein of 1 to 5 dpf *Tg(tagln:NLS-EGFP); Tg(pdgfrb:Gal4FF; UAS:RFP)* zebrafish. (A-E) Maximum intensity projection images of the CA and CV from 1 to 5 dpf. (A'-E') The images from A-E without the brightfield overlay. (F-G) Bar and line graph representations of the number of single- and double-positive cells on the dorsal side of the CA (F), the ventral side of the CA (G), and the CV (H). (I) Schematic diagram illustrating the imaged region. Schematic created with BioRender.com. At least 6 embryos were analyzed at each age. CA, caudal artery. CV, caudal vein. HC, hypochord. NC, notochord. Scale bars: 50 µm.

Figure 5. Low and high *pdgfrb*/*tagln* expression is evident along arterial and venous ISVs from 2 to 5 dpf. (A,B) Maximum intensity projection images of arterial and venous ISVs at 5 dpf. ISVs are outlined by white dotted lines. *tagln*-positive skeletal muscle nuclei are particularly evident in the trunk region near the ISVs, thus requiring frame-by-frame analysis to identify *tagln*-positive perivascular cells. (C,D) Bar graph representations of the number of low and high single- and double-positive cells on the arterial (C) and venous (D) ISVs. Arterial ISVs accumulate *pdgfrb*-high mural cells more

859 robustly than venous ISVs. (E) Representative images of the combinations of *pdgfrb*/*tagln*
860 double-positive cells. (F,G) Bar graph representations of the number double-positive cells
861 on the arterial (F) and venous (G) ISVs. *pdgfrb*/*tagln* double-positive cells were more
862 apparent on arterial ISVs. (H) Schematic diagram summarizing the general localization
863 of perivascular cells on the ISVs at 2 and 5 dpf. *pdgfrb* single-positive cells were more
864 likely to be found on the dorsal ISV region, *tagln* single-positive cells primarily near the
865 notochord ISV region, and double-positive cells nearest to the notochord-neural tube
866 interface by 5 dpf. Schematic created with BioRender.com. At least 6 embryos were
867 analyzed at each age. ISVs, intersegmental vessels. Scale bars for A,B: 50 μm; scale
868 bars for E: 5 μm.
869
870 **Figure 6: Summary of the midline cell populations at the notochord-neural tube**
871 **interface.** We identify the medial floor plate cells as *pdgfrb*/*tagln* double-positive in early
872 zebrafish development (MFP). Additionally, we observe a *tagln* single-positive population
873 of cells along the midline that accumulates below the medial floor plate cells beginning at
874 3 dpf (*tagln*+ Midline Cells). Finally, we describe a mural cell progenitor population near
875 the notochord-neural tube interface that borders either side of the midline. This
876 population—which begins as *tagln* single-positive cells before acquiring *pdgfrb*
877 expression—can be observed migrating to the nearby ISVs from 2 to 5 dpf (MC Progenitor
878 Population). Schematic created with BioRender.com. NC, notochord. NT, neural tube.
879 ISV, intersegmental vessel. MFP, medial floor plate. MC, mural cell.
880
881 **Figure 7. A *tagln*-positive sclerotome-derived mural cell progenitor population at**
882 **the notochord-neural tube interface upregulates *pdgfrb* and migrates to the ISVs.**
883 (A-J) Maximum intensity projection images of cell populations near the notochord-neural
884 tube interface. Sagittal (A,C,E,G,I) and orthogonal (B,D,F,H,J) views of the medial floor
885 plate from 1-5 dpf reveal *pdgfrb*/*tagln* co-expression (cyan arrows). A separate *tagln*
886 single-positive population of cells accumulates immediately below the MFP starting at 3
887 dpf (E-J, white outlined arrows). Finally, an independent *tagln* single-positive population—
888 hereafter the mural cell progenitor population—aligns near the notochord-neural tube
889 interface (A'-I',B,D,F,H,J, yellow arrows) and begins to elongate and upregulate *pdgfrb*

890 over time. (K) Schematic diagram illustrating the three described cell populations from a
891 sagittal and orthogonal view. (L-O) The *tagln*-positive midline cells (white outlined arrows)
892 and mural cell progenitors (yellow arrows) are *twist1a*-positive, indicating they are derived
893 from the sclerotome, unlike the medial floor plate (pink arrows). (P-W) Cells from the
894 mural cell progenitor population can be seen migrating to the ISVs using *pdgfrb* and *tagln*
895 as markers (P-S) or *twist1a* and *tagln* (T-W). ISVs are outlined. White arrows indicate
896 migrating cells. Schematic created with BioRender.com. NC, notochord. NT, neural tube.
897 ISV, intersegmental vessel. MFP, medial floor plate. MC, mural cell. Scale bars: 10 μm.
898

Figure 1

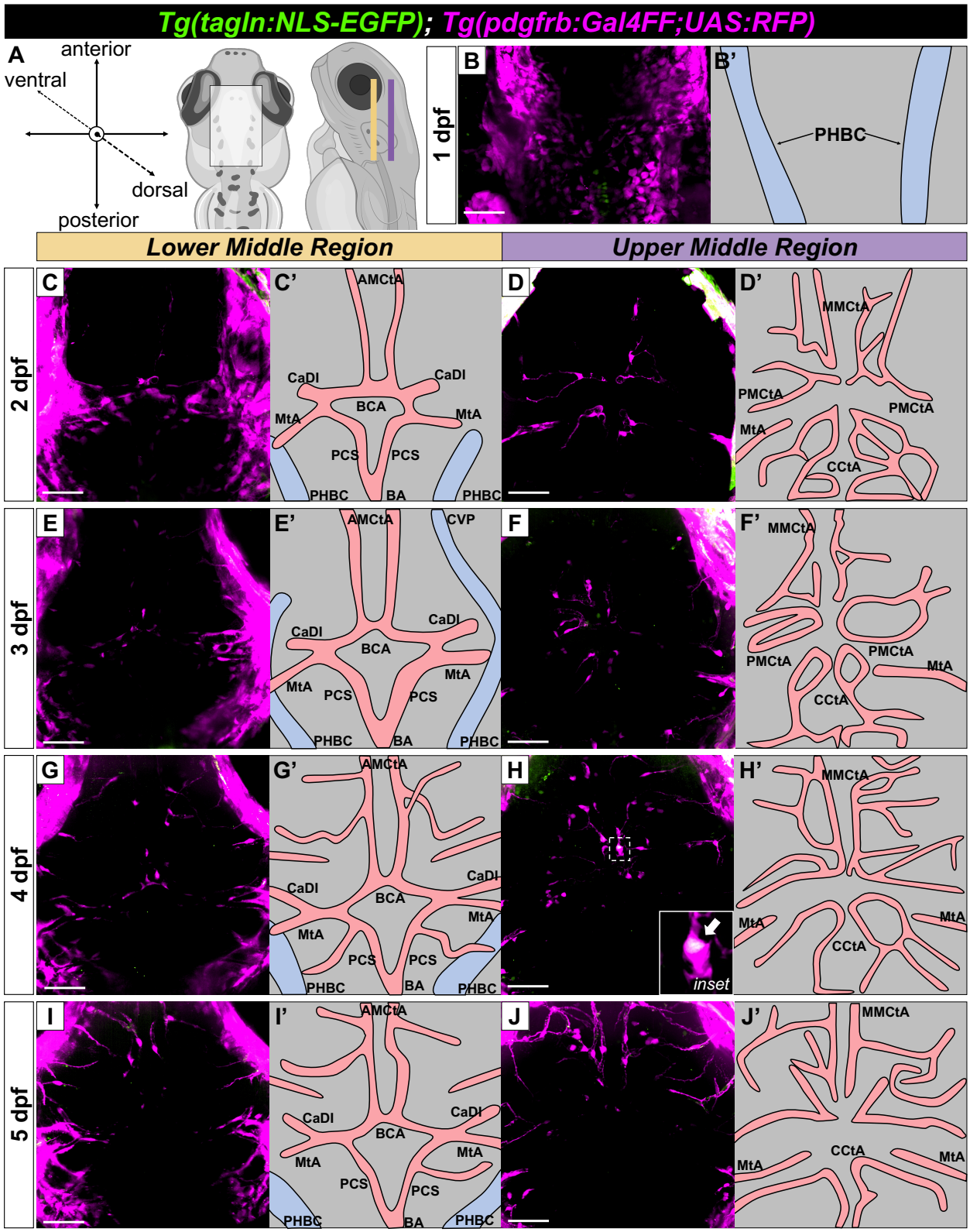
Tg(tagln:NLS-EGFP); Tg(pdgfrb:Gal4FF;UAS:RFP)
A
anterior
ventral
dorsal
posterior
1 dpf
B
B'
PHBC
Lower Middle Region
Upper Middle Region
2 dpf
C
C'
AMCtA
CaDI
CaDI
BCA
MtA
MtA
PCS
PCS
PHBC
BA
PHBC
D
D'
MMCtA
PMCtA
PMCtA
MtA
CCtA
3 dpf
E
E'
AMCtA
CVP
CaDI
CaDI
BCA
MtA
MtA
PCS
PCS
PHBC
BA
PHBC
F
F'
MMCtA
PMCtA
PMCtA
MtA
CCtA
4 dpf
G
G'
AMCtA
CaDI
CaDI
BCA
MtA
MtA
PCS
PCS
PHBC
BA
PHBC
H
inset
H'
MMCtA
MtA
MtA
CCtA
5 dpf
I
I'
AMCtA
CaDI
CaDI
BCA
MtA
MtA
PCS
PCS
PHBC
BA
PHBC
J
J'
MMCtA
CCtA
MtA
MtA

Figure 2

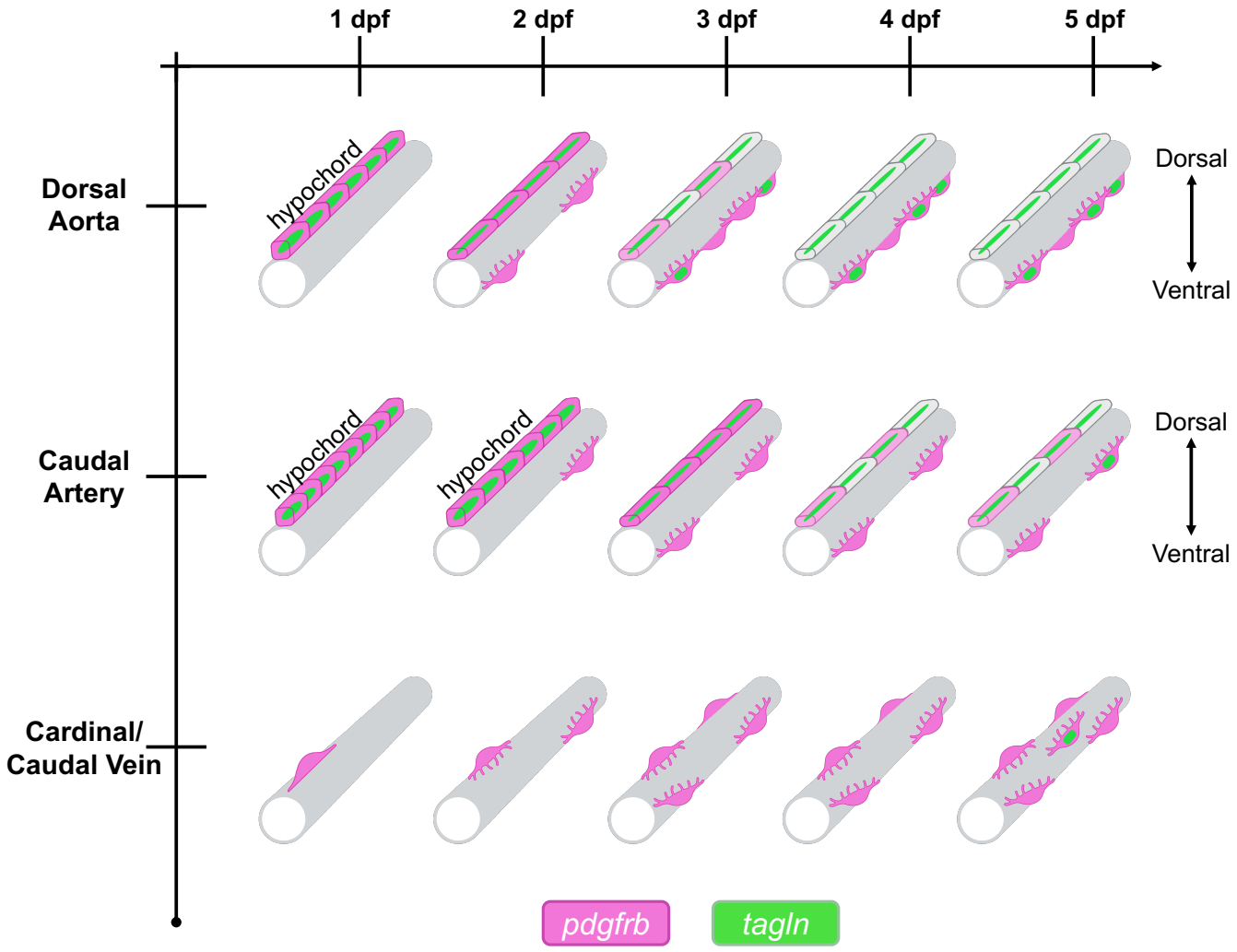
1 dpf
2 dpf
3 dpf
4 dpf
5 dpf
Dorsal Aorta
Caudal Artery
Cardinal/ Caudal Vein
hypochord
hypochord
Dorsal
Ventral
Dorsal
Ventral
pdgfrb
tagln

Figure 3

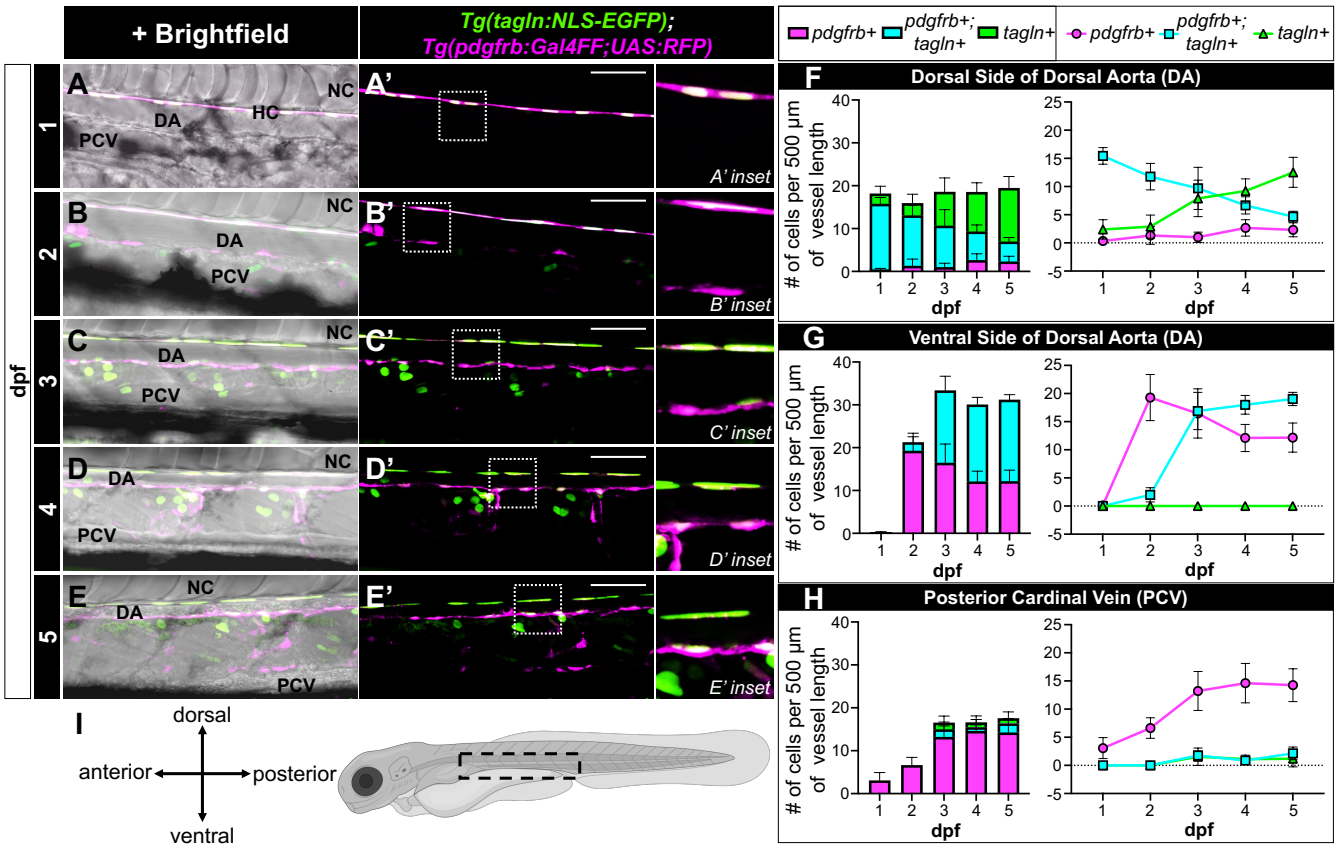
+ Brightfield
Tg(tagln:NLS-EGFP);
Tg(pdgfrb:Gal4FF;UAS:RFP)
dpf
1
2
3
4
5
A
B
C
D
E
NC
HC
DA
PCV
A'
B'
C'
D'
E'
A' inset
B' inset
C' inset
D' inset
E' inset
I
dorsal
anterior
posterior
ventral
pdgfrb+
pdgfrb+; tagln+
tagln+
F
Dorsal Side of Dorsal Aorta (DA)
G
Ventral Side of Dorsal Aorta (DA)
H
Posterior Cardinal Vein (PCV)
# of cells per 500 µm of vessel length
dpf

Figure 4

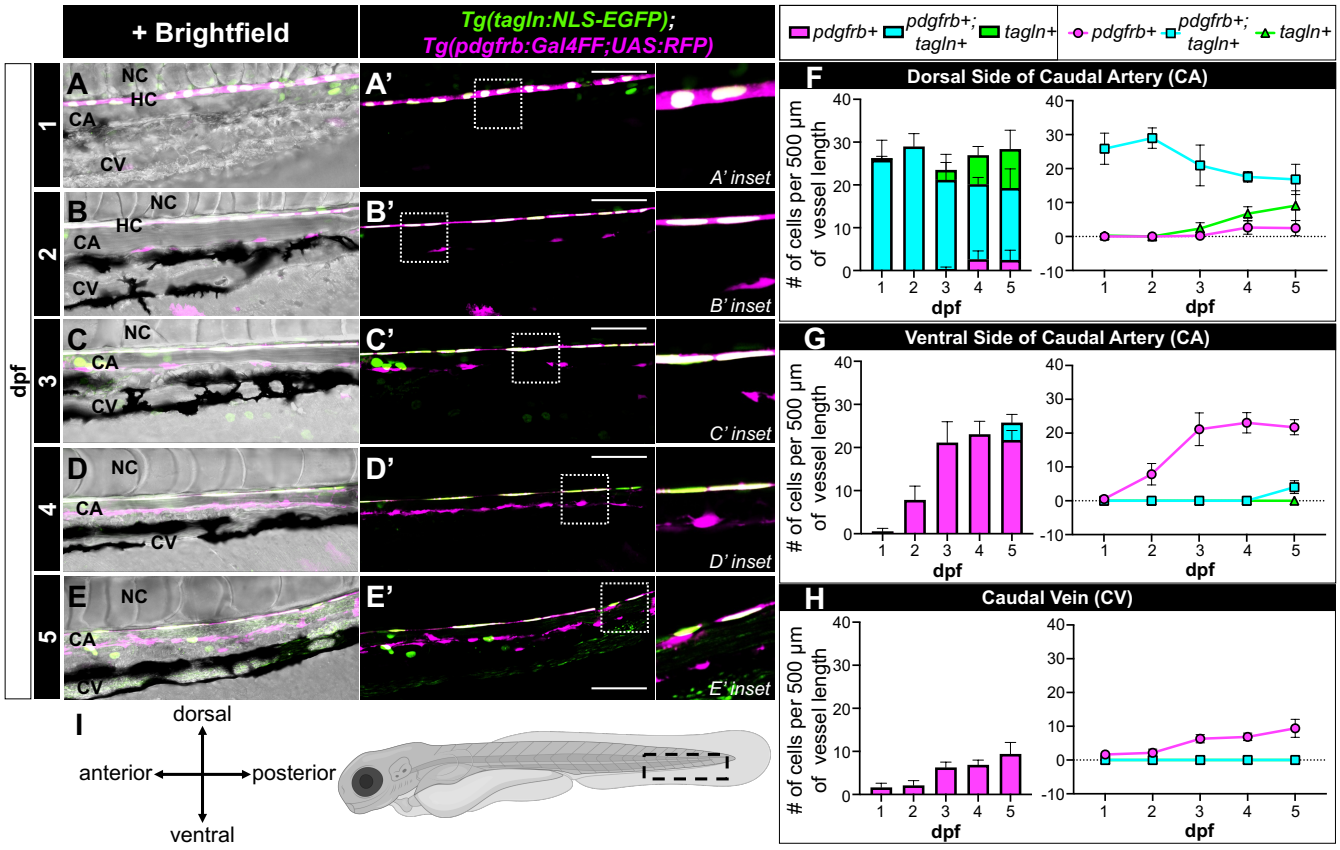
+ Brightfield
Tg(tagln:NLS-EGFP);
Tg(pdgfrb:Gal4FF;UAS:RFP)
pdgfrb+
pdgfrb+; tagln+
tagln+
dpf
NC
HC
CA
CV
A' inset
B' inset
C' inset
D' inset
E' inset
F
Dorsal Side of Caudal Artery (CA)
G
Ventral Side of Caudal Artery (CA)
H
Caudal Vein (CV)
# of cells per 500 µm of vessel length
dpf
I
dorsal
anterior
posterior
ventral

Figure 5

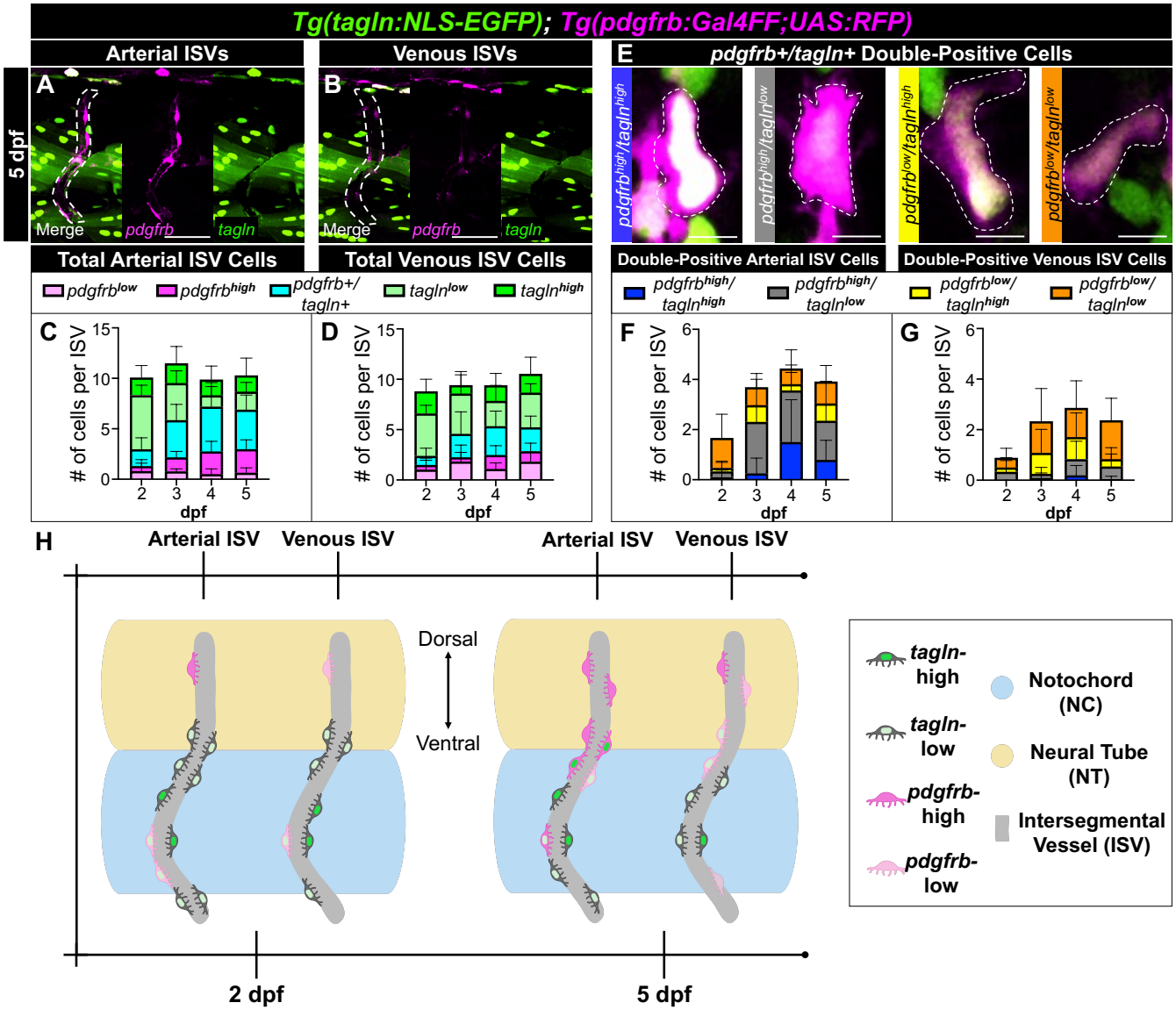
Tg(tagln:NLS-EGFP); Tg(pdgfrb:Gal4FF;UAS:RFP)
Arterial ISVs
Venous ISVs
E
pdgfrb+/tagln+ Double-Positive Cells
5 dpf
A
B
Merge
pdgfrb
tagln
pdgfrbhigh/taglnhigh
pdgfrbhigh/taglnlow
pdgfrblow/taglnhigh
pdgfrblow/taglnlow
Total Arterial ISV Cells
Total Venous ISV Cells
Double-Positive Arterial ISV Cells
Double-Positive Venous ISV Cells
pdgfrblow
pdgfrbhigh
pdgfrb+/tagln+
taglnlow
taglnhigh
pdgfrbhigh/taglnhigh
pdgfrbhigh/taglnlow
pdgfrblow/taglnhigh
pdgfrblow/taglnlow
C
D
F
G
# of cells per ISV
dpf
H
Arterial ISV
Venous ISV
Arterial ISV
Venous ISV
Dorsal
Ventral
2 dpf
5 dpf
tagln-high
tagln-low
pdgfrb-high
pdgfrb-low
Notochord (NC)
Neural Tube (NT)
Intersegmental Vessel (ISV)

Figure 6

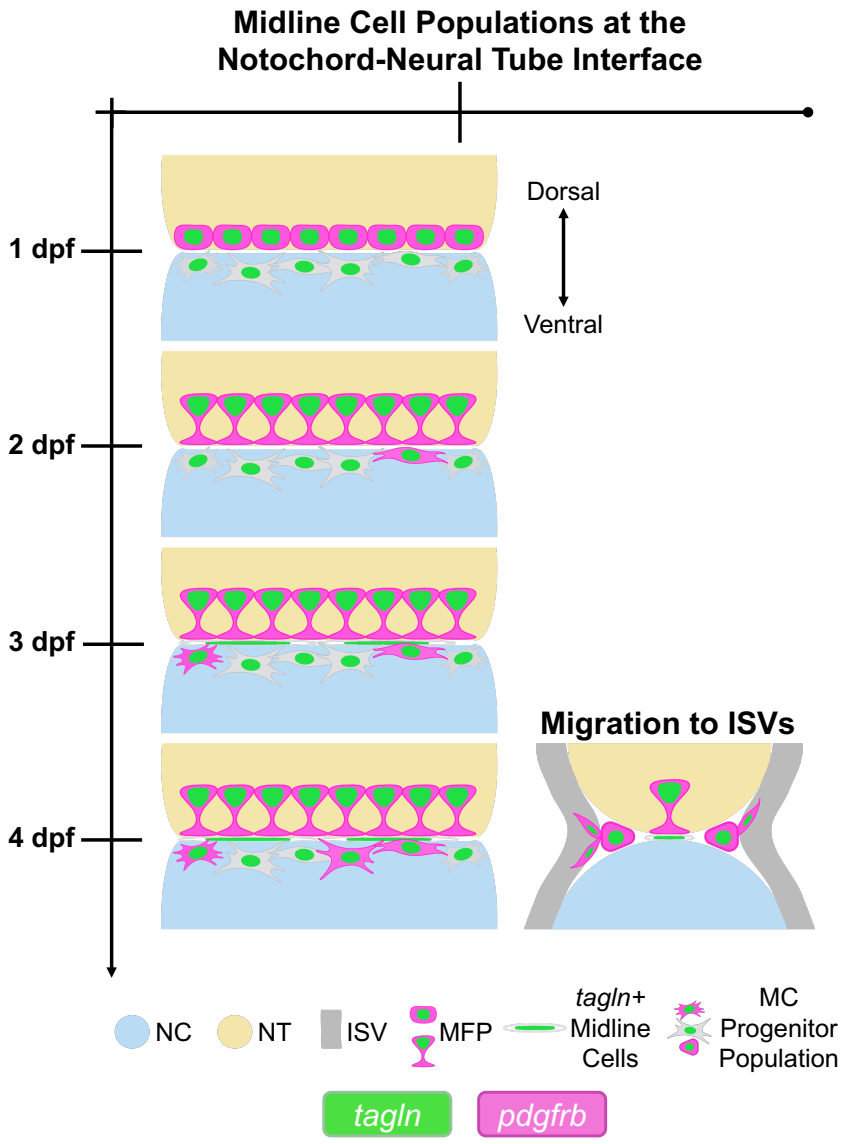
Midline Cell Populations at the
Notochord-Neural Tube Interface
Dorsal
Ventral
1 dpf
2 dpf
3 dpf
4 dpf
Migration to ISVs
NC
NT
ISV
MFP
tagln+
Midline
Cells
MC
Progenitor
Population
tagln
pdgfrb

Figure 7

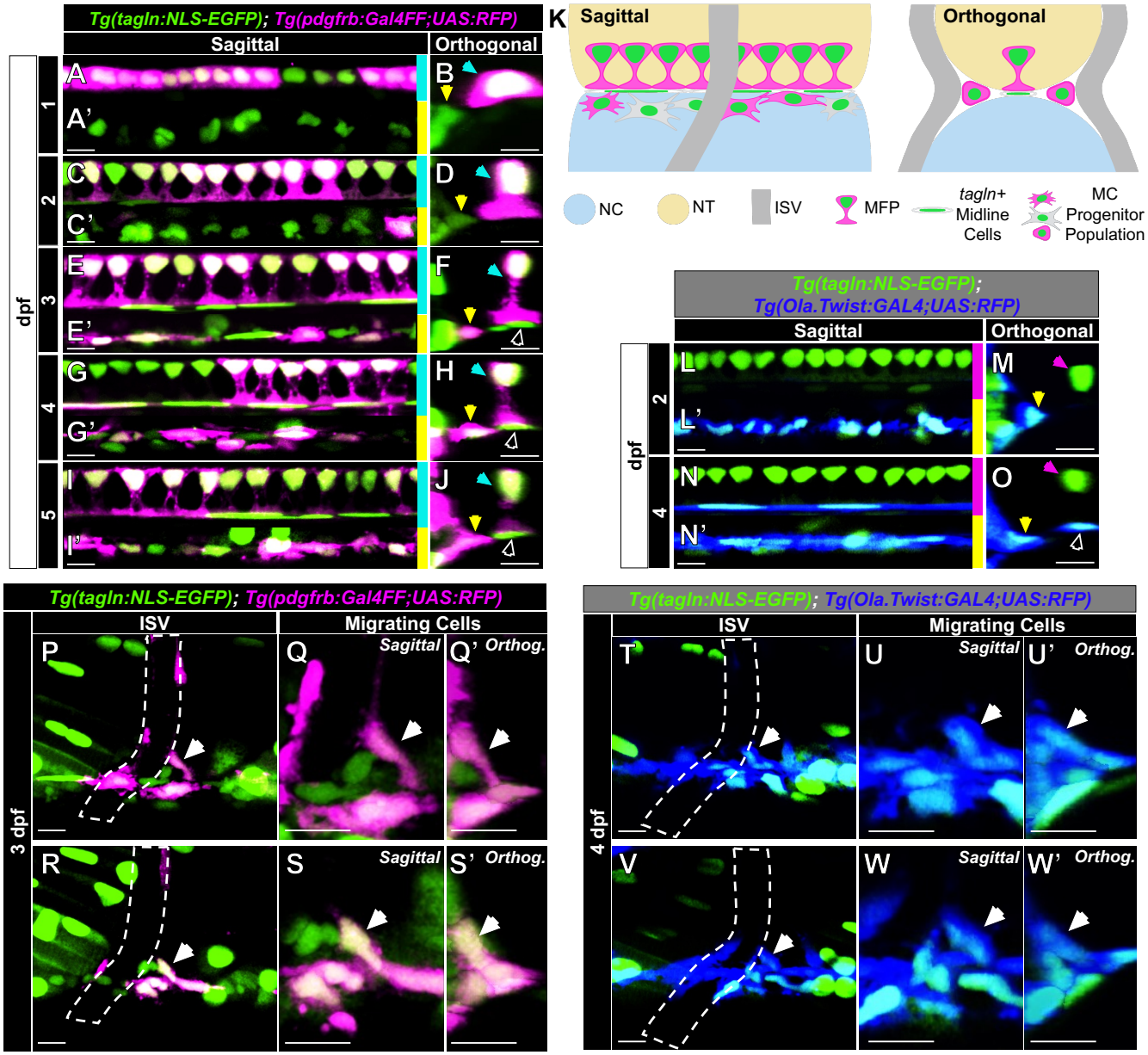
Tg(tagln:NLS-EGFP); Tg(pdgfrb:Gal4FF;UAS:RFP)
Sagittal
Orthogonal
dpf
1
2
3
4
5
A
A'
B
C
C'
D
E
E'
F
G
G'
H
I
I'
J
K
Sagittal
Orthogonal
NC
NT
ISV
MFP
tagln+ Midline Cells
MC Progenitor Population
Tg(tagln:NLS-EGFP); Tg(Ola.Twist:GAL4;UAS:RFP)
Sagittal
Orthogonal
dpf
2
4
L
L'
M
N
N'
O
Tg(tagln:NLS-EGFP); Tg(pdgfrb:Gal4FF;UAS:RFP)
ISV
Migrating Cells
3 dpf
P
Q
Sagittal
Q'
Orthog.
R
S
Sagittal
S'
Orthog.
Tg(tagln:NLS-EGFP); Tg(Ola.Twist:GAL4;UAS:RFP)
ISV
Migrating Cells
4 dpf
T
U
Sagittal
U'
Orthog.
V
W
Sagittal
W'
Orthog.

Supplementary Figure 1

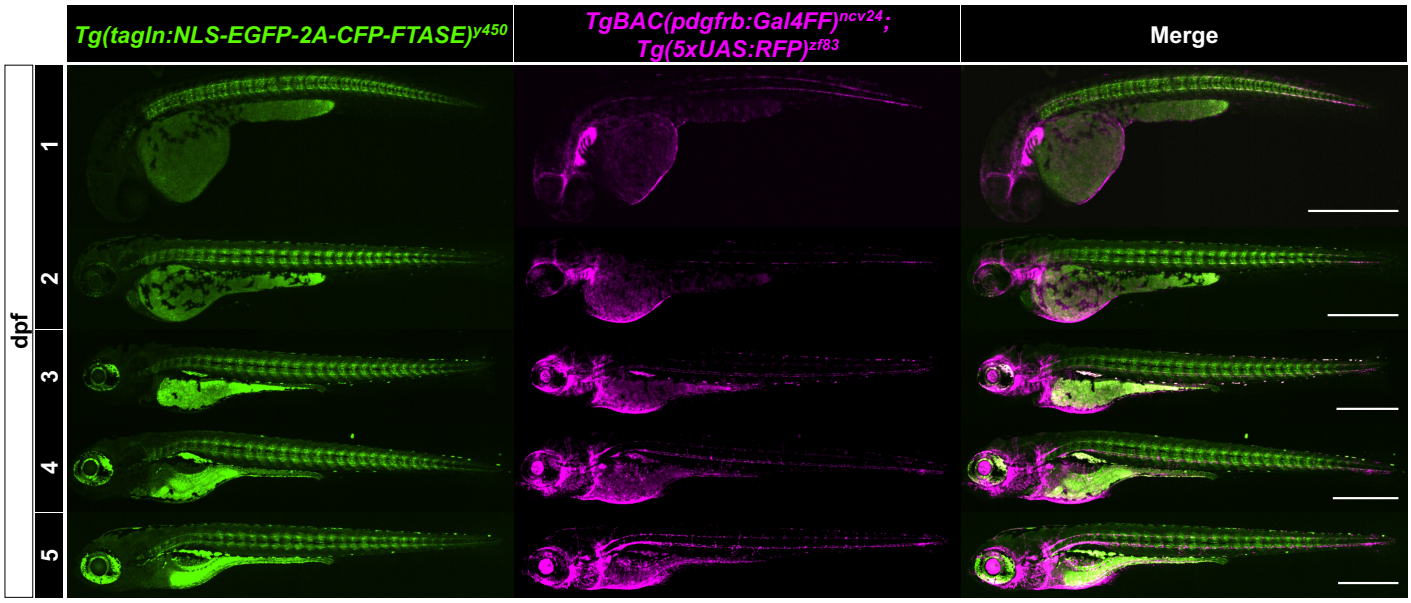

Supplementary Figure 1. *pdgfrb* and *tagln* fluorescent reporter lines. Lateral view confocal images of *Tg(tagln:NLS-EGFP-2A-CFP-FTASE); TgBAC(pdgfrb:Gal4FF); Tg(5xUAS:RFP)* triple transgenic zebrafish embryos from 1-5 dpf. *tagln* expression becomes increasingly evident in the skeletal muscle of the trunk and the intestinal compartment. *pdgfrb* expression is primarily visible in the anterior and cranial regions. Scale bars: 500 μm.

Supplementary Figure 2

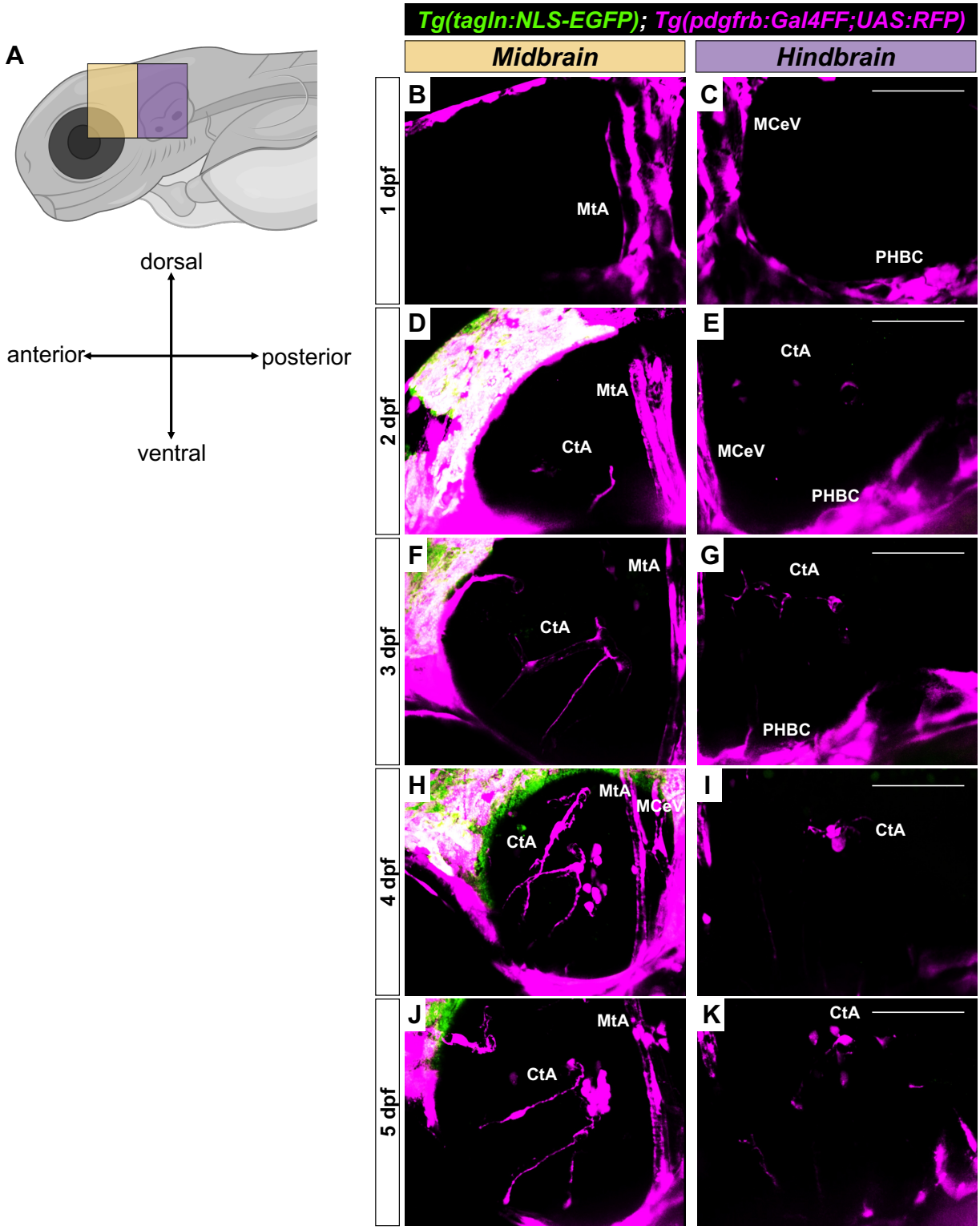

Supplementary Figure 2, Cont.

Supplementary Figure 2. Sagittal views of the mid- and hindbrain of 1 through 5 dpf *Tg(tagln:NLS-EGFP); Tg(pdgfrb:Gal4FF; UAS:RFP)* zebrafish. (A) Schematic diagram illustrating the orientation for imaging sagittal sections of the midbrain (yellow) and hindbrain (purple). (B-K) Maximum intensity projection images of the mid- and hindbrain from 1 to 5 dpf. At 1 dpf (B,C) *pdgfrb*-positive cells are associated with the PHBC, MtA, and MCeV. At 2 dpf (D,E) *pdgfrb*-positive cells begin to accumulate on the CtAs. *pdgfrb*-positive cells continue to accumulate on the CtAs from 3 to 5 dpf (F-K) in both the mid- and hindbrain regions. *tagln*-positive cells were not evident in any of the sagittal images of the mid- or hindbrain. Schematic created with BioRender.com. PHBC, primordial hindbrain channel. MtA, metencephalic artery. MCeV, middle cerebral vein. CtA, central artery. Scale bars: 50 μm.

Supplementary Figure 3

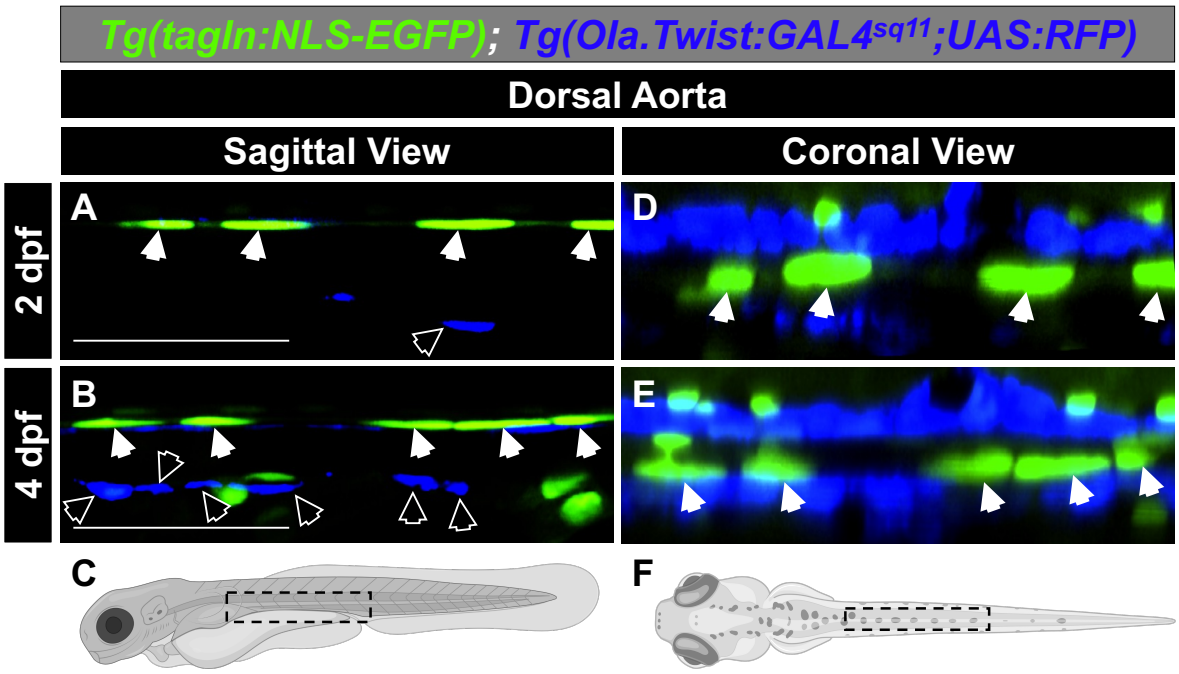

Supplementary Figure 3. *tagln* single-positive cells on the dorsal side of the DA are not sclerotome-derived. Confocal images of the DA in *Tg(tagln:NLS-EGFP); Tg(Ola.Twist:GAL4; UAS:RFP)* fish at 2 dpf (A,D) and 4 dpf (B,E). From the sagittal view (A-C), *tagln*-positive nuclei derived from the hypochord are apparent at 2 dpf and do not express *twist1a* at the 2 or 4 dpf timepoints (solid white arrows), unlike vSMCs on the ventral side of the DA that do express *twist1a* (white outlined arrows). From the coronal view (D-F), *tagln* single-positive nuclei of the hypochord on the dorsal side of the DA are *twist1a*-negative at both time points (solid white arrows), though *twist1a*-positive cells do abut the DA in this region. These data indicate that the *tagln*-single positive hypochord cells on the dorsal side of the DA are not replaced by sclerotome-derived vSMCs after 2 dpf when the hypochord has been previously reported to disappear. (C,F) Schematic diagrams illustrating the orientation for imaging sagittal (C) or coronal (F) sections of the DA. Schematics created with BioRender.com. DA, Dorsal Aorta. Scale bars: 50 μm.

Supplementary Figure 4

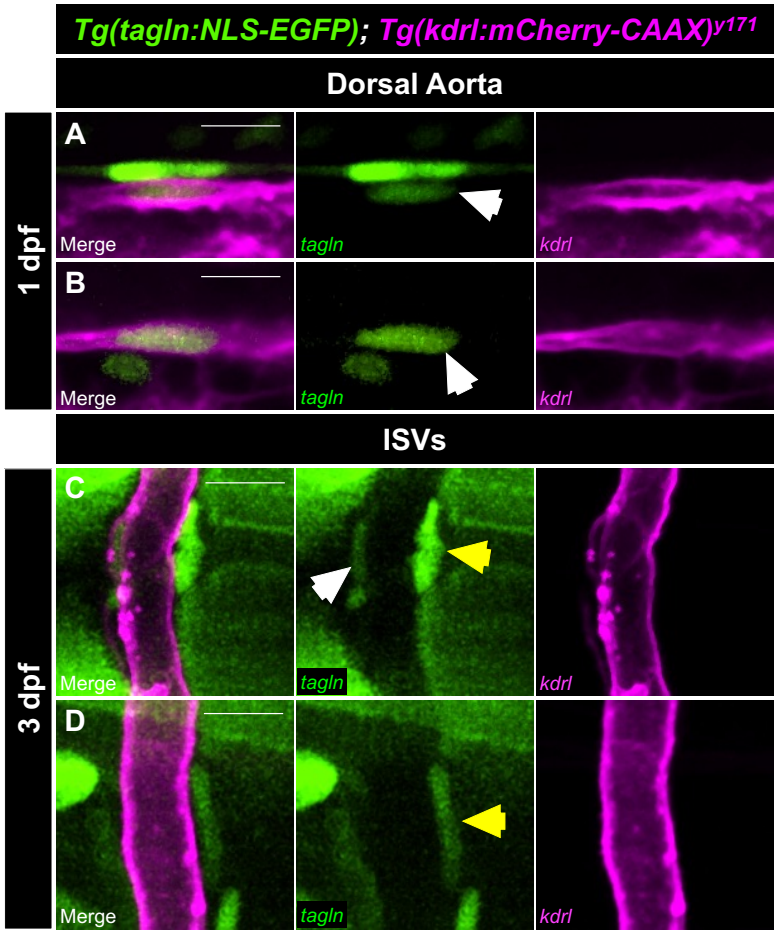

Supplementary Figure 4. Low *tagln* expression is evident in endothelial cells and a subset of perivascular cells on the ISVs. (A-D) Confocal images of *Tg(tagln:NLS-EGFP); Tg(kdrl:mCherry-CAAX)* fish at 1 dpf (A,B) and 3 dpf (C,D) where *kdrl* is used to mark endothelial cells (magenta). (A-C) Low *tagln* expression is seen in endothelial cells of the aorta and ISVs (white arrows). High (C) and low (D) *tagln* expression is also visible in perivascular cells on the ISVs (yellow arrows). Low *tagln* expression in the endothelial cells of the axial vessels is easily distinguishable from high expression in vSMCs, therefore it did not confound the mural cell counts of the axial vessels of *Tg(tagln:NLS-EGFP); Tg(pdgfrb:Gal4FF; UAS:RFP)* fish. However, ISV endothelial cells and *tagln*-low perivascular cells were difficult to distinguish, thus a small number of endothelial cells may be included in the count of *tagln*-low cells of the ISVs. ISVs, intersegmental vessels. Scale bars: 10 μm.

Supplementary Figure 5

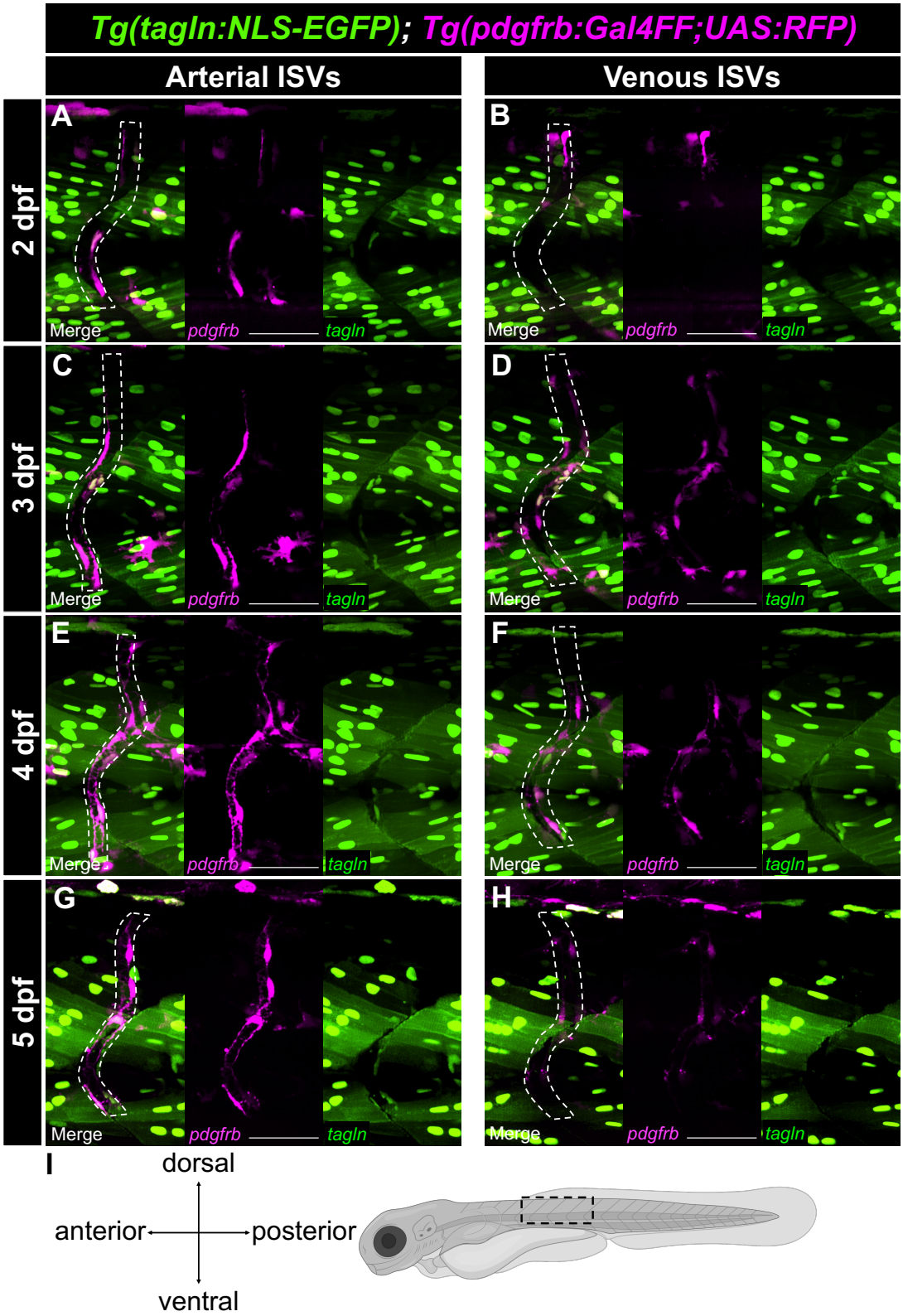

Supplementary Figure 5, Cont.

Supplementary Figure 5. *tagln* and *pdgfrb* expression along arterial and venous ISVs of 2 to 5 dpf *Tg(tagln:NLS-EGFP); Tg(pdgfrb:Gal4FF; UAS:RFP)* zebrafish. (A-H) Maximum intensity projection images of arterial and venous ISVs from 2 to 5 dpf. ISVs are outlined by white dotted lines. *tagln*-positive skeletal muscle nuclei are particularly evident in the trunk region near the ISVs, thus requiring frame-by-frame analysis to identify *tagln*-positive perivascular cells. Arterial ISVs (A,C,E,G) accumulate *pdgfrb*-high mural cells at higher levels than venous ISVs (B,D,F,H). All combinations of low and high *pdgfrb* and *tagln* expression were detected in single- and double-positive perivascular cells surrounding the ISVs at all timepoints, though *pdgfrb/tagln* double-positive cells were more apparent on arterial ISVs. (I) Schematic diagram illustrating the imaged region. Schematic created with BioRender.com. ISVs, intersegmental vessels. Scale bars: 50 μm.

Supplementary Figure 6

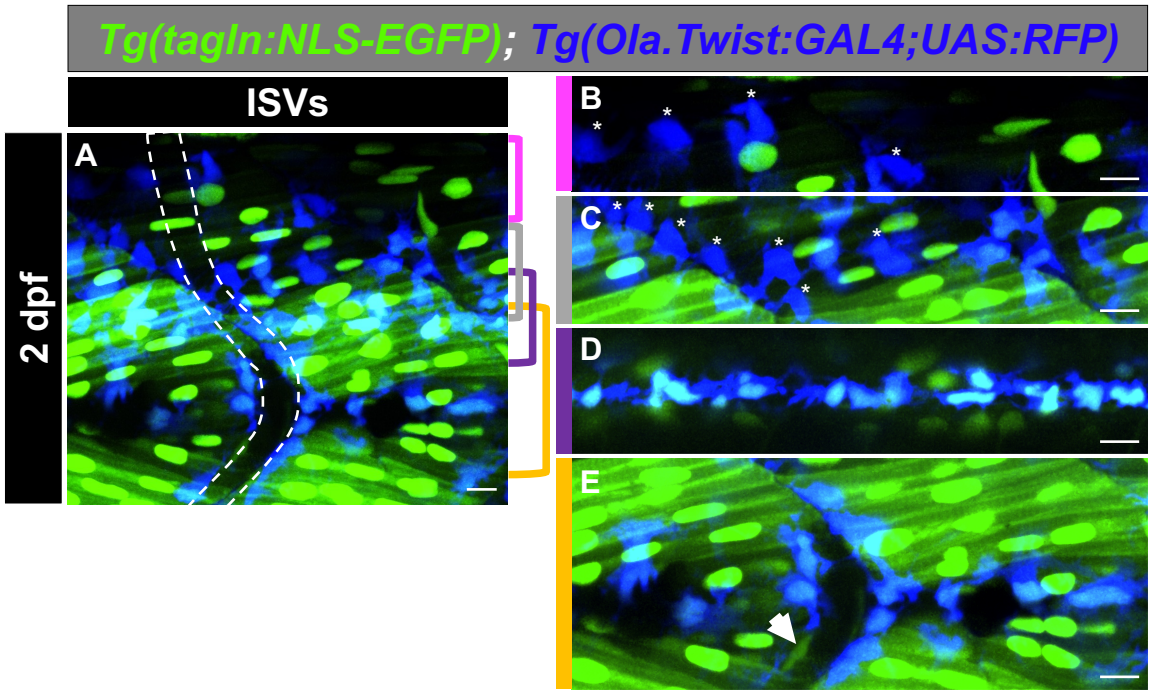

Supplementary Figure 6. Sclerotome-derived cells with low *tagln* expression are predicted to arise from the ventral sclerotome compartment. (A) Maximum intensity projection image of the ISV region of a *Tg(tagln:NLS-EGFP); Tg(Ola.Twist:GAL4; UAS:RFP)* fish at 2 dpf. ISV is outlined with a white dotted line. (B-E) Discrete regions of panel A are max projected for better visualization of *twist1a*-positive cells near the neural tube (B,C), notochord-neural tube interface (D), and notochord (E). The majority of *twist1a*-positive cells near the neural tube are *tagln*-negative (indicated by stars), while all *twist1a*-positive cells at the notochord-neural tube interface and below are *tagln*-positive. Due to the ventral localization of *tagln/twist1a* double-positive cells, we suspect that these cells arise from the ventral sclerotome, with *twist1a*-single positive cells near the neural tube arising from the dorsal sclerotome. The *tagln*-positive/*twist1a*-negative vascular cell in panel E is likely endothelium (white arrow). ISVs, intersegmental vessels. Scale bars: 10 µm.

Supplementary Figure 7

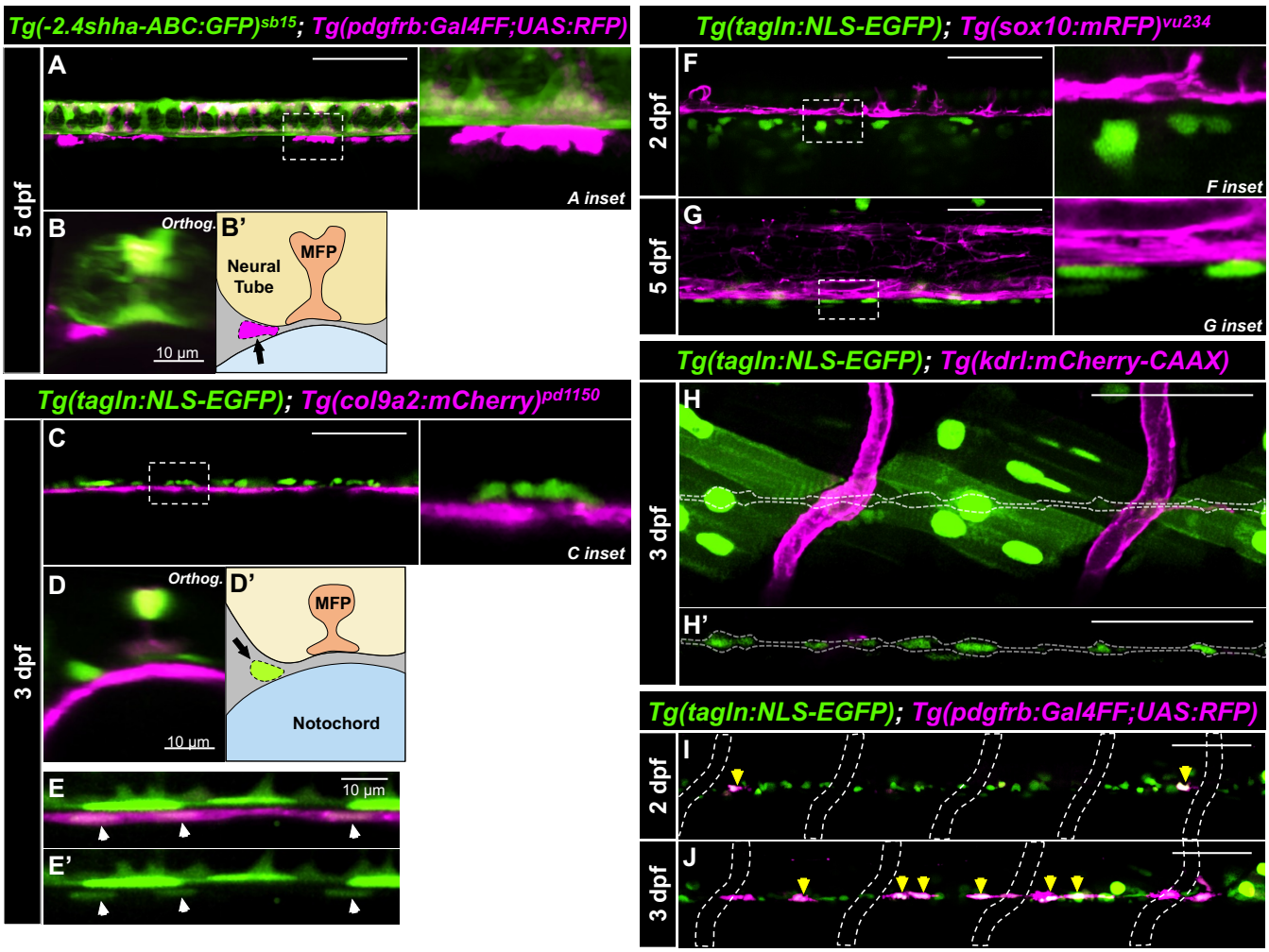

Supplementary Figure 7. The MC progenitor population resides between the notochord and neural tube, is not derived from neural crest, and does not need to contact endothelium to upregulate *pdgfrb*. (A,B) Confocal images of *Tg(-2.4shha-ABC:GFP); Tg(pdgfrb:Gal4FF; UAS:RFP)* zebrafish to visualize the medial floor plate cells (*shha*) and the MC progenitor population (*pdgfrb*) at 5 dpf. The sagittal (A) and orthogonal (B) views show the MC progenitors outside of the neural tube. (B') Schematic detailing the structures in panel B. (C-E) Confocal images of *Tg(tagln:NLS-EGFP); Tg(col9a2:mCherry)* zebrafish to visualize the notochord sheath cells (*col9a2*) and the MC progenitor population (*tagln*) at 3 dpf. The sagittal (C) and orthogonal (D) views show the MC progenitors outside of the notochord. (D') Schematic detailing the structures in panel D. (E,E') Notochord sheath cells (white arrows) express low levels of *tagln*. (F,G) Confocal images of *Tg(tagln:NLS-EGFP); Tg(sox10:mRFP)* fish to visualize the neural crest (*sox10*) and the MC progenitor population (*tagln*) at 2 dpf (F) and 5 dpf (G). MC progenitor cells do not overlap with neural crest populations. (H) Confocal images of *Tg(tagln:NLS-EGFP); Tg(kdrl:mCherry-CAAX)* fish to visualize endothelial cells (*kdrl*) and the MC progenitor population (*tagln*) at 3 dpf. The MC progenitor population (outlined with a white dotted line) is not adjacent to a blood vessel. (H') Z-stack slice showing the MC progenitor population from panel H without the skeletal muscle. (I,J) Confocal images of *Tg(tagln:NLS-EGFP); Tg(pdgfrb:Gal4FF; UAS:RFP)* fish at 2 dpf (I) and 3 dpf (J). ISVs are outlined with white dotted lines. MC progenitor cells upregulate *pdgfrb* expression (yellow arrows) without contact with the endothelium. MC, mural cell. MFP, medial floor plate. Scale bars: 50 µm unless otherwise indicated.

Supplementary Figure 8

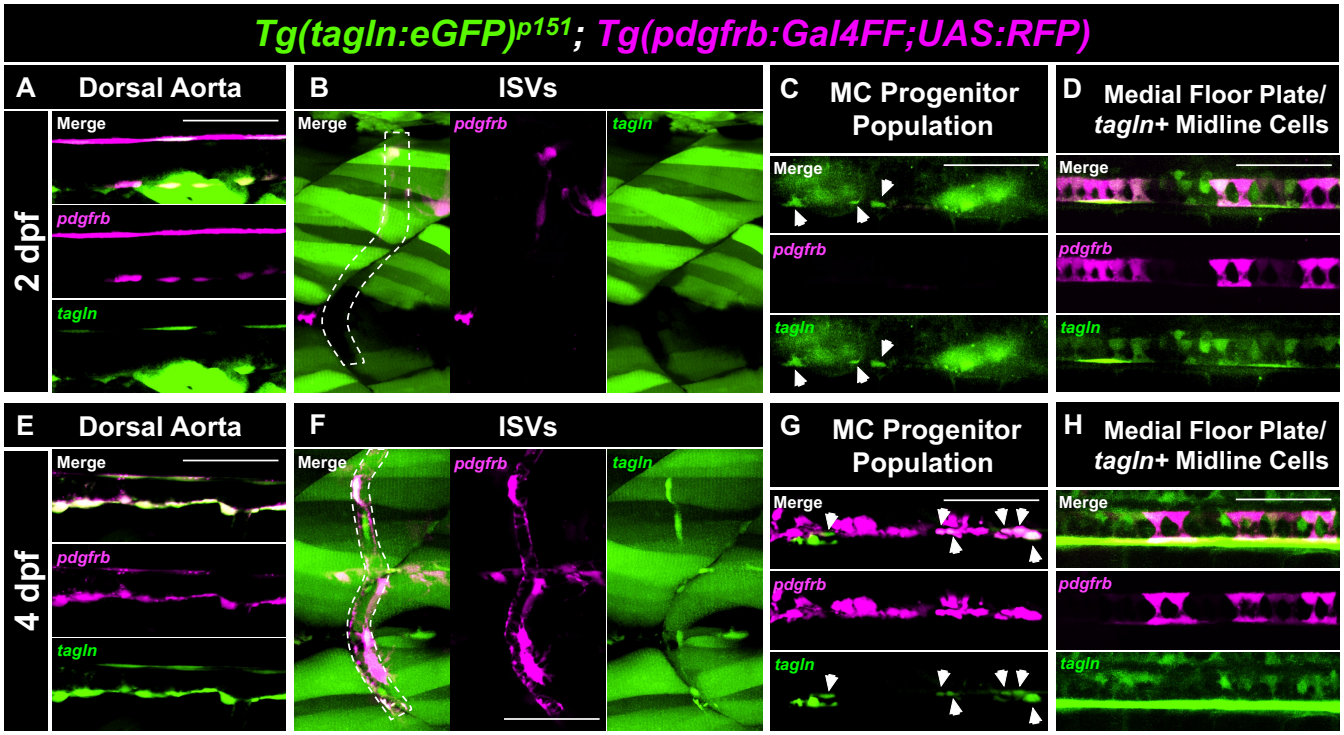

Supplementary Figure 8. Visualizing *tagln* expression using a cytosolic-GFP *tagln* reporter line. Confocal images of *Tg(tagln:eGFP); Tg(pdgfrb:Gal4FF; UAS:RFP)* fish at 2 dpf (A-D) and 4 dpf (E-H). *tagln* expression was evident in the hypochord and vSMC populations of the dorsal aorta (A,E), though GFP signal was more easily detectable in vSMCs than the hypochord. GFP expression in the skeletal muscle decreased the efficiency and resolution of identifying *tagln*-positive cells in the trunk, though we were able to visualize *tagln*-high mural cells on the ISVs by 4 dpf (B,F). Despite high background, GFP signal was also detectable in the MC progenitor population and the medial floor plate cells (C,D,G,H). We observed intense GFP expression in the *tagln*-positive midline cells by 4 dpf (H). Thus, we were able to confirm *tagln* expression in these structures using an independent transgenic, the cytosolic-GFP *tagln* reporter. MC, mural cell. ISVs, intersegmental vessels. Scale bars: 50 μm.

Movies 1, 2, 3

Movie 1. A 3D view of *pdgfrb* and *tagln* expression in the hypochord between 1 to 4 dpf. Movie of rotating 3D projections. Projections were made from confocal z-stacks of the hypochord in *Tg(tagln:NLS-EGFP); Tg(pdgfrb:Gal4FF; UAS:RFP)* zebrafish. *pdgfrb* expression decreased between 1-4 dpf, while cells of the hypochord elongated and decreased slightly in number, as evidenced by the change in shape and number of *tagln*-positive nuclei. Scale bar: 50 µm.

Movie 2. 3D views of MC progenitor cells migrating to the ISVs in *Tg(tagln:NLS-EGFP); Tg(pdgfrb:Gal4FF; UAS:RFP)* zebrafish at 3 dpf. Movie of two rotating 3D projections, side by side. Projections were made from confocal z-stacks of the MC progenitor population identified by *pdgfrb* and *tagln* expression. Arrows point to the migrating cells. ISVs are outlined by white dotted lines. Scale bar: 10 µm.

Movie 3. 3D views of MC progenitor cells migrating to the ISVs in *Tg(tagln:NLS-EGFP); Tg(Ola.Twist:GAL4; UAS:RFP)* zebrafish at 4 dpf. Movie of two rotating 3D projections, side by side. Projections were made from confocal z-stacks of the MC progenitor population identified by *twist1a* and *tagln* expression. Arrows point to the migrating cells. ISVs are outlined by white dotted lines. Scale bar: 10 µm.